

Positronium and heavy quarkonia as testing case for discretized light-cone quantization

M. Krautgärtner, H. C. Pauli, and F. Wölz

Max-Planck-Institut für Kernphysik, D-6900 Heidelberg, Germany

(Received 17 June 1991; revised manuscript received 6 December 1991)

A nonperturbative method for solving quantum field theories in three space and one time dimensions is applied to the bound-state problem of positronium and heavy quarkonia. The model includes only one dynamical photon, i.e., the irradiation channels are closed. An integral equation of the Bethe-Salpeter type is derived, being the light-cone analogue of the Tamm-Dancoff equation, and solved numerically. The model accounts for the Bohr-Sommerfeld and Dirac physics such as hyperfine splitting including the correct retardation. Special emphasis is put on the role of the Coulomb singularity in momentum space. Numerical results for the mass spectrum and the wave functions are presented, and compared to analytical results. Agreement is found for the physical value of the coupling constant. For very large coupling constants $\alpha \sim 0.3$ discrepancies are noted and discussed.

PACS number(s): 11.10.Ef, 11.10.Qr, 11.15.Tk

I. INTRODUCTION

In recent years the method of discretized light-cone quantization [1] (DLCQ) has been tested successfully for one space and one time dimension by its application to Yukawa theory [2], quantum electrodynamics [3,4], and quantum chromodynamics [5]. The perspective to develop this method in three space and one time dimensions into a tool of comparable efficiency is rather exciting and worth an effort. In this work, we shall report on some progress, albeit one has not solved yet all the problems of a fundamental or technical nature.

DLCQ as a method is based on the Hamiltonian formalism in the light-cone gauge $A^+ = 0$, in which all particles are physical, quantizing the system at equal light-cone time $x^+ = t + z$ rather than at usual time t [6,7]. The light-cone gauge might actually generate problems [8], but they have probably no impact on the questions to be discussed below. The method as it stands [9,10] is potentially able to generate solutions to gauge field theory in the real world of three space and one time dimensions. We refer to Tang, Brodsky, and Pauli [9] for a fairly complete account of the preceding work, for the treatment of ultraviolet and infrared regularization and subsequent renormalization, and for problems with gauge invariance and their solution in the presence of a sharp momentum cutoff.

The methods and approximations should be tested thoroughly by explicit calculations, before tackling the true challenge, namely, the solutions of non-Abelian gauge theory in $3+1$ dimensions. The present work was undertaken with the aim of providing such a test. In $3+1$ dimensions no soluble models exist, unfortunately, which are both physical and tractable. One faces head-on the true physical problems, and thus we have to address ourselves in this paper to the nonperturbative solution of $(3+1)$ -dimensional QED (QED_{3+1}), in particular to the bound-state problem for positronium at strong coupling ($\alpha \approx 0.3$). The test is successful if one is able to generate numerically the correct Bohr spectrum, the wave func-

tions, the fine and hyperfine structure [11] including recoil effects [12], and possibly even the Lamb shift, in this order of numerical relevance. Restricting the test to QED_{3+1} and positronium, one has the great advantage of comparing to a large body of analytical work [11,12]. It should be emphasized strongly that the present work should not be misunderstood as competitive in either quality or precision.

We solve positronium in a very simple model, as formulated in Sec. II: Only one dynamical photon is included in the Fock-space expansion. The annihilation channel of two photons is omitted, as well as the single-photon state which in principle couples into the orthopositronium. Model positronium is thus perfectly stable, cannot irradiate into two photons and bears a great similarity to "muonium with equal masses." Despite its simplicity, the model should cover all of Bohr-Sommerfeld and Dirac physics such as, for example, the Bohr scales and the hyperfine splitting including the correct retardation. At this level of approximation, QED and QCD are identical to the extent that substituting $\alpha_{\text{el-mag}} \Rightarrow \frac{4}{3}\alpha_{\text{strong}}$ generates the corresponding QCD solutions rigorously. The positronium results can thus be transliterated to the heavy quarkonia such as charmonium.

While this work was going on, also with respect to developing the technology, several works of Wilson and co-workers [13] have appeared, which consider the same model *in abstracto*. For good reasons, they stress the point that Tamm [14] and Dancoff [15] did approach field theory many years ago in very much the same spirit as we do it. We therefore shall refer to the model of including only one dynamical photon as the *light-cone Tamm-Dancoff approach*.

As we are abusing a physical problem as a test for a numerical method, one faces the familiar problem of such an approach: One is constantly in danger of mistaking a technological error as a new physical effect. In the earlier work [9], for example, the vain attempts to generate numerically stable results in line with expectation have been rather frustrating. Only when realizing that the good old

Coulomb singularity was present in a light-cone Hamiltonian formalism also, of course, did these difficulties fade away. For this reason, comparatively broad room is devoted to the ‘‘Coulomb trick’’ in Sec. III, treating the nonrelativistic Coulomb problem in the momentum representation on its own merit.

The major part of this work deals with a careful specification of the model, leaving out eventually all details which could be found in Ref. [9]. But much effort has been devoted to developing the technology, including the symmetries discussed in Sec. IV, which ultimately has lead to an amazingly effective numerical approach. One is able to see the essential physics already when diagonalizing a 25×25 matrix. This simplicity provides the potential for treating more complicated models in the future.

Unfortunately, as discussed in Sec. V, the formalism is not yet developed sufficiently well to establish an approximate independence of the results on formal parameters such as the covariant momentum cutoff at sufficiently large coupling constants. As we plan to discuss the related problems in forthcoming work (II), the present work can be only an intermediate step.

II. DERIVING THE LIGHT-CONE TAMM-DANCOFF EQUATION

In discretized light-cone quantization [9] (DLCQ) the generalized momentum operators P^μ are a discrete and covariant realization of the Heisenberg operators which propagate the system in space-time, i.e., $i\partial_\mu\psi = [\psi, P_\mu]$. Their Lorentz-invariant contraction $H_{\text{LC}} = P^\mu P_\mu$ is discrete and frame independent, and is called the *light-cone Hamiltonian*. Upon diagonalization

$$H_{\text{LC}}|\psi_i\rangle = \tilde{M}_i^2|\psi_i\rangle, \quad (2.1)$$

it delivers the (stationary) eigenfunctions $|\psi_i\rangle$ and eigenvalues \tilde{M}_i^2 which have the dimension of an invariant mass squared. For QED₃₊₁ their derivation as Fock-space operators can be found elsewhere [9,10] together with the complete tables of the Hamiltonian matrix elements. Some of the latter are compiled in Appendix B.

In the sequel we proceed the way we think DLCQ should be applied. One formulates the model in a discretized momentum basis, where the Hamiltonian can be visualized as a matrix with a finite number of rows and columns. Next, one formulates all necessary model assumptions, in accord with covariance and gauge invariance, and finally by going over to the continuum limit one converts the matrix equation to an integral equation. Finally, one solves the integral equations with suitably optimized numerical methods. It should be emphasized that the regularization scheme of DLCQ [9] explicitly allows for such a procedure, since the regularization scales are equal both for discretization and the continuum, contrary to lattice gauge theory, for example.

A. The formulation of the model

As part of the model we restrict ourselves to the charge-zero sector and include only the *electron-positron*

($e\bar{e}$) and the *electron-positron-photon* ($e\bar{e}\gamma$) Fock states, denoted collectively by $|e\bar{e}\rangle$ and $|e\bar{e}\gamma\rangle$, respectively. It is convenient to introduce them as projectors, i.e., $Q_0 \equiv \sum_i |(e\bar{e})_i\rangle\langle(e\bar{e})_i|$ and $Q_1 \equiv \sum_i |(e\bar{e}\gamma)_i\rangle\langle(e\bar{e}\gamma)_i|$. The index i runs over the discrete light-cone momenta and helicities of the partons (electron e , positron \bar{e} , and photon γ) subject to fixed total momenta and to covariant regularization by a sharp momentum cutoff. Occasionally, we shall refer to Q_0 and Q_1 as P - and Q -space, respectively. The one-boson model was recently investigated also by Kaluža [16] and by Hollenberg *et al.* [17].

The Hamiltonian matrix equation, Eq. (2.1), can then be understood as a coupled matrix equation involving the block matrices $H_{nn'} \equiv Q_n H_{\text{LC}} Q_{n'}$:

$$\begin{aligned} H_{00}|\psi\rangle_0 + H_{01}|\psi\rangle_1 &= \omega|\psi\rangle_0, \\ H_{10}|\psi\rangle_0 + H_{11}|\psi\rangle_1 &= \omega|\psi\rangle_1, \end{aligned} \quad (2.2)$$

with $\omega \equiv \tilde{M}_i^2$ and the projected eigenfunctions $|\psi\rangle_n \equiv Q_n|\psi\rangle$. Quite in general, by introducing inverse matrices or resolvents $G(\omega) \equiv 1/(\omega - H)$, one can express $|\psi\rangle_1$ in terms of $|\psi\rangle_0$ from the latter of the above equations, i.e.,

$$|\psi\rangle_1 = \frac{1}{\omega - H_{11}} H_{10}|\psi\rangle_0, \quad (2.3)$$

and insert it into the first one. Eventually, Eq. (2.1) can be identically rewritten in terms of an ‘‘effective Hamiltonian’’ acting only in P -space: i.e.,

$$H_{\text{eff}}(\omega)|\psi_i(\omega)\rangle_0 = \tilde{M}_i^2(\omega)|\psi_i(\omega)\rangle_0, \quad (2.4)$$

with

$$H_{\text{eff}}(\omega) \equiv H_{00} + H_{01} \frac{1}{\omega - H_{11}} H_{10}.$$

Once the P -space eigenfunction $|\psi_i(\omega)\rangle_0$ is known, one can calculate $|\psi\rangle_1$ from Eq. (2.3) by a quadrature. The projection technique of deriving an effective Hamiltonian is fairly standard in many-body theory [18], and has been applied to light-cone formulation before, both implicitly [6] and with explicit mentioning [19]. Apart from a different model (gauge theory instead of Yukawa), different regularization and a different space-time parametrization (equal light-cone time instead of equal time), the model is the light-cone analogue of the Tamm-Dancoff approach [14,15]. A similar approach was applied recently [20] also to QED with scalar fields.

The effective Hamiltonian H_{eff} depends on the unknown eigenvalue ω through the resolvent (‘‘energy denominator’’). To solve it in principle, one starts, for example, with some fixed value ω as the ‘‘starting point energy,’’ inverts $(\omega - H_{\text{LC}})$ in Q -space, calculates and subsequently diagonalizes H_{eff} in P -space to get the eigenvalues $\tilde{M}_i^2(\omega)$. The true eigenvalues are determined by variation of ω and the fixed-point equation $\omega = \tilde{M}_i^2(\omega)$. An alternative and very elegant method to solve the equations has also been formulated by Tamm [14]. Despite acting only in the smaller P -space Eq. (2.4) is thus not necessarily simpler to solve than the full problem. But Eq. (2.4) can be approximated easier than Eq.

(2.1). This cannot be done without a closer look on the explicit structure of the matrices.

A restriction to any finite number of gauge bosons violates gauge invariance, and one has to correct for it. In order to avoid that scattering amplitudes are gauge violated already on the tree level, Tang, Brodsky, and Pauli [9] have formulated a “gauge cutoff,” namely to include the instantaneous interactions only when the “instantaneous parton” is accompanied by a real “dynamic parton” with the same spacelike momentum and in the same Fock-space configuration. As an example, consider instantaneous interactions which occur in Q -space, as illustrated in Fig. 1. Diagram (a) has to be excluded, since there are no $|e\bar{e}\gamma\gamma\rangle$ Fock states in the model, as well as diagram (b) since the two-photon states are absent. Thus, only diagram (d) survives the gauge cutoff.

For discussing further the effective Hamiltonian, the electron and the positron are characterized by their four-momenta k_e^μ and $k_{\bar{e}}^\mu$, respectively, their Lagrangian mass m_F , and their helicities. More explicitly, as displayed in Fig. 2, the electron is described by $k_e^\mu = (x, \mathbf{k}_\perp, k_e^-)$, i.e., its longitudinal-momentum fraction $x = k_e^+ / P^+$, its transverse momentum \mathbf{k}_\perp , its energy $k_e^- = (m_F^2 + \mathbf{k}_\perp^2) / x$, and finally by its spin projection s_e . Correspondingly, the positron is described by $k_{\bar{e}}^\mu = (1-x, -\mathbf{k}_\perp, k_{\bar{e}}^-)$, and $s_{\bar{e}}$. The effective Hamiltonian is written as the sum of the diagonal kinetic energy $M_{e\bar{e}}^2 \equiv (k_e + k_{\bar{e}})^2$ and the effective interaction $V_{\text{eff}}(\omega)$, which both have the dimension of an invariant mass squared, i.e.,

$$H_{\text{eff}}(\omega) = M_{e\bar{e}}^2 + V_{\text{eff}}(\omega), \quad (2.5)$$

with

$$V_{\text{eff}}(\omega) = C + S + V_{01} \frac{Q_1}{\omega - M_{e\bar{e}}^2 + S_{q\bar{q} \rightarrow q\bar{q}}^{(a)}} V_{10}.$$

The effective interaction contains thus the diagonal contraction terms C in P -space, the seagull interaction $S = S_{q\bar{q} \rightarrow q\bar{q}}^{(s)}$ in P -space, and the iterated vertex interaction in which $V_{01} = H_{01}$ connects P -space with Q -space through the vertex graph $V_{q \rightarrow qg}$. The energy denominator is not diagonal due to the matrix element $S_{qg \rightarrow qg}^{(a)}$. The effective interaction “scatters” an $e\bar{e}$ pair from a state $(k_e, k_{\bar{e}})$ into another state $(k'_e, k'_{\bar{e}})$, which in general

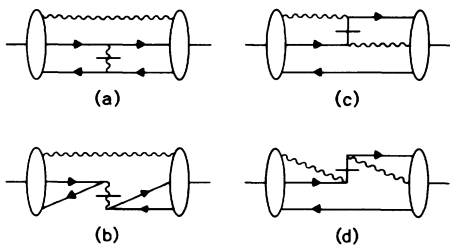


FIG. 1. The instantaneous interactions in Q -space. (a) and (b): the instantaneous boson interactions $S_{q\bar{q} \rightarrow q\bar{q}}^{(s)}$ and $S_{q\bar{q} \rightarrow q\bar{q}}^{(a)}$, respectively. (c) and (d): the instantaneous fermion interactions $S_{qg \rightarrow qg}^{(s)}$ and $S_{qg \rightarrow qg}^{(a)}$, respectively.

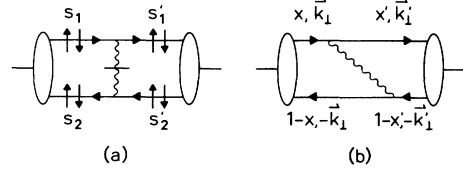


FIG. 2. The off-diagonal matrix element in P -space. (a) the instantaneous boson graph $S_{q\bar{q} \rightarrow q\bar{q}}^{(s)}$; (b) the iterated graph $W = VGV$. The figure displays also the spacelike momentum assignment of the fermions; those of the boson are fixed by momentum conservation. (b) holds for $x > x'$, the corresponding one for $x < x'$ is not shown.

has a different invariant mass. Their average $\omega^* = \frac{1}{2}(k_e + k_{\bar{e}})^2 + \frac{1}{2}(k'_e + k'_{\bar{e}})^2$, i.e.,

$$\omega^* \equiv \frac{1}{2}(k_e^- + k_{\bar{e}}^- + k'_e^- + k'_{\bar{e}}^-) = \frac{1}{2} \left[\frac{m_F^2 + \mathbf{k}_\perp^2}{x(1-x)} + \frac{m_F^2 + \mathbf{k}'_\perp{}^2}{x'(1-x')} \right], \quad (2.6)$$

being introduced for later convenience, will be referred to as the symmetrized mass (squared).

As part of the model *two ad hoc assumptions* are made in the sequel, namely to substitute the eigenvalue by the symmetrized mass and to omit diagram in Fig. 1(d), i.e.,

$$\omega \Rightarrow \omega^* \quad \text{and} \quad S_{qg \rightarrow qg}^{(a)} = 0. \quad (2.7)$$

Supposedly, the first of them accounts approximately for the violation of gauge invariance by including only one dynamical photon. Note that the effective interaction is then independent of the eigenvalue. The second is suggested only by mathematical simplification. The Q -space matrix is then diagonal and can be inverted trivially. Note that the same assumptions have been made in all of the preceding work [6,14,15,19]. This model is solved with rigor, numerically.

B. The singularity structure of the effective interaction

Investigating the effective interaction V_{eff} , one should distinguish between the *off-diagonal* matrix elements displayed in Fig. 2 and the *diagonal* elements with $x = x'$ and $\mathbf{k}_\perp = \mathbf{k}'_\perp$ in Fig. 3. In the discretized case, this is always possible. The diagonal element $V_{\text{eff}}(\omega) = C + W(\omega)$ vanishes strictly due to mass renormalization, as shown in some detail in Appendix A. The off-diagonal part $V_{\text{eff}}(\omega) = S + W(\omega)$ seems to have the collinear singularity at $x = x'$ due to the instantaneous interaction $S = S_{q\bar{q} \rightarrow q\bar{q}}^{(s)}$. But as shown next, it cancels against terms in $W(\omega)$. The cancellation can be verified either by inserting directly the explicit matrix elements in Appendix B, or, more transparently, in terms of four-vectors [7,10]. In Fig. 2 one deals with four-vectors: namely, the momentum transfer of the electron $l_e^\mu \equiv (k'_e - k_e)^\mu$, the momentum transfer of the positron $l_{\bar{e}}^\mu \equiv (k_{\bar{e}} - k'_{\bar{e}})^\mu$, and the photon momentum $q^\mu = (q, \mathbf{q}_\perp, q^-)$, with $q \equiv q^+ / P^+$. Using the lightlike vector [6] $\eta^\mu = (0, 0, 0, 2)$ they are related by

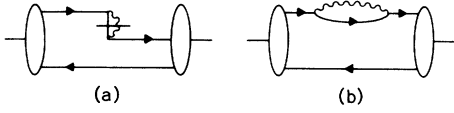


FIG. 3. The diagonal matrix elements in P -space. (a) the instantaneous contraction terms, (b) the iterated graph $W = VGV$ (self-mass diagram).

$$q^\mu = l_e^\mu + \frac{1}{2}\eta^\mu(q^- + l_e^-) = l_{\bar{e}}^\mu + \frac{1}{2}\eta^\mu(q^- + l_{\bar{e}}^-). \quad (2.8)$$

Because of momentum conservation, the three have the same spacelike components, but their timelike component is different. It is also useful to introduce a modified energy denominator as an always positive number and to rewrite it in terms of the four-momentum transfers and the symmetrized mass squared ω^* , i.e.,

$$\begin{aligned} \mathcal{D} &\equiv -q(\omega - M_{e\bar{e}\gamma}^2) \\ &= |x - x'|(\omega^* - \omega) - \frac{1}{2}l_e^2 - \frac{1}{2}l_{\bar{e}}^2. \end{aligned} \quad (2.9)$$

Next, evaluate the iterated vertex graph Fig. 2 according to the rules [10]. With the electron current $j(l_e)^\mu \equiv \bar{u}(k_e')\gamma^\mu u(k_e)$ and the positron current $j(l_{\bar{e}})^\nu \equiv \bar{u}(k_{\bar{e}}')\gamma^\nu u(k_{\bar{e}})$ one gets

$$W(\omega) = -(g^2/\mathcal{D})j(l_e)^\mu j(l_{\bar{e}})^\nu d_{\mu\nu}.$$

The polarization sum of the photons $d_{\mu\nu} \equiv \sum_\lambda \epsilon(\lambda, q)_\mu \epsilon(\lambda, q)_\nu^*$, yielding [6]

$$d_{\mu\nu} = -g_{\mu\nu} + (1/q)(q_\mu \eta_\nu + q_\nu \eta_\mu),$$

obviously contains a gauge-dependent part. As one wants to apply the identity $(k_e' - k_e)_\mu \bar{u}(k_e')\gamma^\mu u(k_e) = 0$, one substitutes the photon momentum q^μ once by l_e^μ and once by $l_{\bar{e}}^\mu$; thus,

$$d_{\mu\nu} = -g_{\mu\nu} - l_{e\mu}\eta_\nu - l_{\bar{e}\nu}\eta_\mu + (1/2q)\eta_\mu\eta_\nu(2q^- + l_e^- + l_{\bar{e}}^-).$$

One ends up with

$$\begin{aligned} W(\omega) &= \frac{g^2}{\mathcal{D}}j(l_e)^\mu j(l_{\bar{e}})_\mu \\ &\quad - \frac{g^2}{2\mathcal{D}q}j(l_e)^\mu j(l_{\bar{e}})^\nu \eta_\mu\eta_\nu(2q^- + l_e^- + l_{\bar{e}}^-). \end{aligned} \quad (2.10)$$

When evaluating the instantaneous graph in Fig. 2(a) according to the rules [10], i.e.,

$$S_{q\bar{q} \rightarrow q\bar{q}}^{(s)} = g^2 \frac{1}{q^2} j(l_e)^\mu j(l_{\bar{e}})^\nu \eta_\mu \eta_\nu, \quad (2.11)$$

one notes the similarity with the gauge-dependent part of Eq. (2.10). Adding the two, using the discrepancy function

$$\Delta \equiv \frac{1}{2} \left[\frac{2\mathcal{D}}{q} - 2q^- - l_e^- - l_{\bar{e}}^- \right],$$

thus

$$\Delta = \omega^* - \omega,$$

and the definition $j(l_e)^\mu \eta_\mu = j_e^+$, the effective interaction becomes finally

$$V_{\text{eff}}(\omega) = \frac{g^2}{\mathcal{D}}j(l_e)^\mu j(l_{\bar{e}})_\mu + \frac{g^2}{\mathcal{D}} \frac{\Delta}{|x - x'|} j_e^+ j_{\bar{e}}^+. \quad (2.13)$$

The photon energies q^- explicitly cancel. The remaining singularity in $\Delta/|x - x'|$ vanishes in the present model, see Eq. (2.7). By *fiat*, the effective potential has thus no ultraviolet or infrared singularities. Only the usual integrable Coulomb singularity remains.

C. The light-cone Tamm-Dancoff equation

In the continuum, the matrix equation (2.4) becomes an integral equation

$$\left[\frac{m_F^2 + \mathbf{k}_1^2}{x(1-x)} - \tilde{M}_i^2 \right] \psi(x, \mathbf{k}_1, s_e, s_{\bar{e}}) + \sum_{s_e', s_{\bar{e}}'} \int_D dx' d^2 \mathbf{k}'_1 \langle x, \mathbf{k}_1; s_e, s_{\bar{e}} | V_{\text{eff}}(\omega) | x', \mathbf{k}'_1; s_e', s_{\bar{e}}' \rangle \psi(x', \mathbf{k}'_1, s_e', s_{\bar{e}}') = 0. \quad (2.14)$$

The finite domain of integration D is set by covariant Fock-space regularization [9]:

$$\frac{m_F^2 + \mathbf{k}_1^2}{x(1-x)} \leq \Lambda^2 + 4m_F^2, \quad (2.15)$$

with given cutoff scale Λ . Combined with Eq. (2.7) we shall speak of this equation as the ‘‘light-cone Tamm-Dancoff’’ equation.

One has to evaluate the sixteen matrix elements $\langle s_e, s_{\bar{e}} | V_{\text{eff}} | s_e', s_{\bar{e}}' \rangle$ for the different helicity combinations in terms of the longitudinal and transversal momenta. As an example, we display the helicity-conserving element, i.e.,

$$\begin{aligned} \langle x, \mathbf{k}_1; \uparrow, \downarrow | V_{\text{eff}}(\omega) | x', \mathbf{k}'_1; \uparrow, \downarrow \rangle &= -\frac{\alpha}{2\pi^2} \frac{1}{\mathcal{D}} \left[m_F^2 \left[\frac{1}{x'x} + \frac{1}{(1-x')(1-x)} \right] + \frac{\mathbf{k}_1 \cdot \mathbf{k}'_1 - i\mathbf{k}_1 \wedge \mathbf{k}'_1}{x'x} + \frac{\mathbf{k}_1 \cdot \mathbf{k}'_1 + i\mathbf{k}_1 \wedge \mathbf{k}'_1}{(1-x')(1-x)} \right. \\ &\quad \left. + \frac{\mathbf{k}_1^2}{x(1-x)} + \frac{\mathbf{k}'_1^2}{x'(1-x')} + \frac{2\Delta}{|x - x'|} \right]. \end{aligned} \quad (2.16)$$

The denominator reads explicitly

$$\begin{aligned} D = & + \frac{m_F^2}{2} (x - x')^2 \left[\frac{1}{xx'} + \frac{1}{(1-x)(1-x')} \right] \\ & + (\mathbf{k}_\perp - \mathbf{k}'_\perp)^2 \\ & - \frac{1}{2} (x - x') \left[\frac{\mathbf{k}_\perp^2}{x} - \frac{\mathbf{k}_\perp^2}{1-x} + \frac{\mathbf{k}'_\perp^2}{1-x'} - \frac{\mathbf{k}'_\perp^2}{x'} \right] \\ & + |x - x'| (\omega^* - \omega), \end{aligned} \quad (2.17)$$

with $\Delta = \omega^* - \omega = 0$, according to Eq. (2.7).

D. The light-cone and the Coulomb Schrödinger equation

The DLCQ matrix equation is approximated by the Tamm-Dancoff equation, Eq. (2.14). In the nonrelativistic limit [$\mathbf{k}_\perp^2 \ll m_F^2$ and $(x - \frac{1}{2})^2 \ll 1$], the latter and particularly Eq. (2.16) is easily converted into the ‘‘light-cone Schrödinger equation’’:

$$\begin{aligned} & \frac{m_F^2 + \mathbf{k}_\perp^2}{x(1-x)} \psi(x, \mathbf{k}_\perp) \\ & - \frac{\alpha}{2\pi^2} \int_D dx' d^2\mathbf{k}'_1 \frac{8m_F^2 \psi(x', \mathbf{k}'_1)}{4m_F^2 (x - x')^2 + (\mathbf{k}'_1 - \mathbf{k}_\perp)^2} \\ & = \tilde{M}^2 \psi(x, \mathbf{k}_\perp), \end{aligned} \quad (2.18)$$

as given in Ref. [6]. One should note, however, that this equation is kind of a hybrid since the nonrelativistic limit is taken only in the potential energy. Therefore, it cannot yield the precise Bohr spectrum. Being merely of numerical interest, one may ask, for example, how much it deviates. This was not done before. When the nonrelativistic limit is taken consistently by replacing the longitudinal-momentum fraction with a ‘‘parallel momentum’’ $k_\parallel \equiv 2m_F(x - \frac{1}{2})$, collecting the momenta into a three-vector $\mathbf{k} = (k_\parallel, \mathbf{k}_\perp)$, substituting the kinetic energy $(m_F^2 + \mathbf{k}_\perp^2)/x(1-x)$ by $4m_F^2 + 4\mathbf{k}^2$, and using the definition $\tilde{M}^2 \equiv 4m_F^2 + 4m_F E$, one arrives straightforwardly at the usual Coulomb Schrödinger equation in momentum space: i.e.,

$$\frac{\mathbf{k}^2}{2m_r} \psi(\mathbf{k}) - \frac{\alpha}{2\pi^2} \int_D d^3\mathbf{k}' \frac{1}{(\mathbf{k} - \mathbf{k}')^2} \psi(\mathbf{k}') = E \psi(\mathbf{k}), \quad (2.19)$$

including the correct reduced mass $m_r = m_F/2$. Fock space regularization converts itself into a three-momentum cutoff; i.e., the domain of integration D is given by $\mathbf{k}^2 \leq \Lambda^2/4$.

The nonrelativistic equations will be studied on their own merit, with the expected results. But they approximate the full equation *only for small* α . As will be seen below, the solutions start to become numerically stable as a function of Λ only when the latter is a multiple of the Bohr momentum, or when $\Lambda = Cm_F\alpha$ with say $C \sim 3$. This leads to the inequality $|\mathbf{k}| \leq \frac{1}{2}\Lambda \ll m_F$, and thus to the condition $\alpha \ll 2/3$. For the value $\alpha = 0.3$ used below, the condition is violated.

E. Recalling the analytical results

Which results should one expect? In an expansion up to order α^4 , the singlet and the triplet mass (excluding annihilation) is given by [11]

$$M_s = 2 - \frac{1}{4}\alpha^2 \left(1 + \frac{63}{48}\alpha^2\right)$$

and (2.20)

$$M_t = 2 - \frac{1}{4}\alpha^2 \left(1 - \frac{1}{48}\alpha^2\right),$$

respectively, where (as in the following) masses are given in units of the physical electron mass. Rather than dealing with the directly calculated invariant masses squared, we shall tabulate below the singlet and triplet *binding coefficients* B , as for example, defined by $B_s \equiv 4(2 - M_s)/\alpha^2$. For $\alpha = 1/137$, the numerical value is very close to 1. Even for $\alpha = 0.3$ they differ only little, i.e., $B_s = 1.118$ and $B_t = 0.998$. The singlet to triplet mass difference will be given in the form of the *hyperfine coefficient* $C_{\text{hf}} \equiv (M_t - M_s)/\alpha^4$. The Fermi value of the hyperfine coefficient is then $(C_{\text{hf}})_{\text{Fermi}} = \frac{1}{3}$, independent of α . Bodwin, Yennie, and Gregorio [12] summarize the analytical work on the hyperfine shift in positronium by

$$\begin{aligned} C_{\text{hf}} = & \frac{1}{2} \left[\frac{2}{3} \left(+ \frac{1}{2} \right) - \frac{\alpha}{\pi} (\ln 2 + \frac{16}{9}) \right. \\ & \left. + \frac{5}{12} \alpha^2 \ln \frac{1}{\alpha} + K \alpha^2 + K' \alpha^3 \right]. \end{aligned} \quad (2.21)$$

The term $\frac{1}{2}$ is set in parentheses since it originates from the photon annihilation term. Not much is known about K' , except that it is stabilized by a $\ln \alpha$ term; it is set to zero. The impact of the coefficient K is very small; its numerical value [12] is $K = +0.427$. Eq. (2.21) predicts therefore the values $C_{\text{hf}} = 0.333$ for $\alpha = \frac{1}{137}$ and $C_{\text{hf}} = 0.257$ for $\alpha = 0.3$.

III. SOLVING NUMERICALLY THE COULOMB EQUATIONS IN MOMENTUM SPACE

Investigating the bound-state problem for QED one is confronted sooner or later with the nonrelativistic Coulomb problem. Since its analytical solutions are known precisely, one might wish to use them for testing and optimizing the computational methods, when trying to solve the momentum-space equation numerically on its own merit. Momentum-space [21] approaches have no difficulty with the center-of-mass problem, and seem to be a powerful tool for solving, for example, the many-body problem (as done for one space dimension [22]) for an arbitrary particle number.

A. The Coulomb singularity

For simplicity, the problem is reduced to treating the rotationally invariant s states. Integrating over the angular variables, Eq. (2.19) gets, with $p \equiv |\mathbf{k}|$,

$$\frac{p^2}{2m_r}\psi(p) + \frac{\alpha}{2\pi} \int_{D_1} dp' \frac{p'}{p} \ln \frac{(p-p')^2}{(p+p')^2} \psi(p') = E\psi(p). \quad (3.1)$$

One is faced with a Fredholm integral equation of the second kind. If the kernel is continuous, the problem can also be solved numerically with the so-called Nyström method [23,24]. This means that one evaluates the integrals with Gaussian quadratures [25] and considers the whole equation at the abscissa points $p=p_i$ to get a finite-dimensional eigenvalue problem. Using Bohr units (note: $\dim[E] \equiv Ry = m_r c^2 \alpha^2 / 2$) the integral equation becomes a matrix equation, i.e.,

$$p_i^2 \psi(p_i) + \frac{1}{\pi} \sum_{j=1}^N \omega_j^{(N)} \frac{p_j}{p_i} \ln \frac{(p_i-p_j)^2}{(p_i+p_j)^2} \psi(p_j) = E\psi(p_i) \quad (3.2)$$

with $\omega_j^{(N)}$ as the Gaussian weights.

It is obvious that the procedure fails in $p_j=p_i$, since the diagonal matrix element of the interaction is not defined. The origin of this difficulty can be traced to the *Coulomb singularity* at $\mathbf{k}=\mathbf{k}'$ in Eq. (2.19). One way of regularizing the equation is to omit simply the diagonal element, i.e., to omit the contribution $j=i$ in the sum of Eq. (3.2). A physical argument could be that the point $\mathbf{k}=\mathbf{k}'$ corresponds to the exchange of a photon with spacelike momentum zero. But treating the equation this way, one gets an amazingly poor convergence as a function of N , the number of integration points included. This is illustrated in Fig. 4, where the convergence to the exact eigenvalues $E_n = -1/n^2$ is virtually absent. Even for a value as large as $N=128$ the discrepancy of the lowest eigenvalues amounts to roughly 15%, as can be seen from Table I. The poor convergence is not caused primarily by the infinite range of the Coulomb potential (or by the zero mass of the photon). Actually, we have done the same type of calculations with a finite photon mass. The diagonal element becomes then finite and well defined, but convergence is not dramatically improved. One has to conclude that the poor convergence cannot have a physical, but must have a mathematical reason.

B. The remedy: Include counterterms

To specify reasonable diagonal elements the integrability of the Coulomb potential can be used. One adds two terms in Eq. (3.2) which cancel each other in the continu-

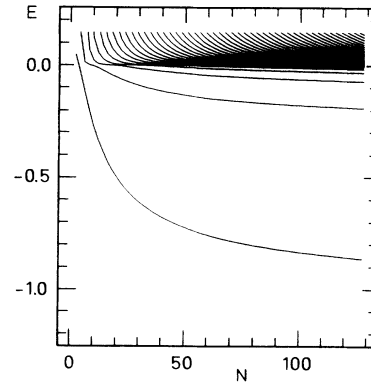


FIG. 4. The eigenvalues of the s states for the Coulomb Schrödinger equation vs the number of integration points N . No measures are taken for the Coulomb singularity. Note the very slow convergence of the bound states with increasing N .

um limit. One of them contains an integral of exactly the same type as before but with the wave function taken at constant abscissa points p_i and with an additional convergence generating function $g(p, p')$, satisfying $g(p, p) = 1$. The other one is just the discretization of that integral; thus,

$$\begin{aligned} p_i^2 \psi(p_i) + \frac{1}{\pi} \sum_{j=1}^N \omega_j^{(N)} \frac{p_j}{p_i} \ln \frac{(p_i-p_j)^2}{(p_i+p_j)^2} \psi(p_j) \\ + \left[-\frac{1}{\pi} \sum_{j=1}^N \omega_j^{(N)} \frac{p_j}{p_i} \ln \frac{(p_i-p_j)^2}{(p_i+p_j)^2} g(p_i, p_j) \right. \\ \left. + \frac{1}{\pi} \int_{D_1} dp' \frac{p'}{p_i} \ln \frac{(p_i-p')^2}{(p_i+p')^2} g(p_i, p') \right] \psi(p_i) \\ = E\psi(p_i). \quad (3.3) \end{aligned}$$

According to the known ground-state function, one chooses

$$g(p, p') = \frac{(1+p^2)^2}{(1+p'^2)^2}. \quad (3.4)$$

Now, because of the opposite sign, the singularity drops out of the sums. The remaining integral will be evaluated analytically, with the result $-\pi(1+p_i^2)$. It does not de-

TABLE I. Lowest bound states of the nonrelativistic Coulomb potential $V = -\alpha/r$. The energy levels are given in units of $mc^2\alpha^2/2$ and the number of integration points is $N = 128$.

Equation (3.2)	$\Lambda = 10$	$\Lambda = \infty$	Exact	n
-0.8546	-0.9970	-1.0000	-1.0000	1
-0.1875	-0.2496	-0.2500	-0.2500	2
-0.0694	-0.1110	-0.1111	-0.1111	3
-0.0309	-0.0625	-0.0625	-0.0625	4
-0.0146	-0.0400	-0.0400	-0.0400	5
-0.0068	-0.0278	-0.0278	-0.0278	6
-0.0028	-0.0204	-0.0204	-0.0204	7
-0.0009	-0.0157	-0.0157	-0.0156	8

pend on the wave function ψ and the occurrent singularities are irrelevant. One should emphasize that the analytical integrability of the integral is most important. Evaluating it numerically should be done with high precision. In practice it is sufficient to integrate p' over a finite interval $[0, \Lambda]$. When the regulator Λ is sufficiently large ($\Lambda \geq 10$), the impact of the convergence generating function $g(p, p')$ is negligible; i.e., it suffices to choose $g(p, p') \equiv 1$. For completeness we mention that after substituting $\psi(p_i) \equiv \phi(p_i) / \sqrt{\omega_i p_i}$ the Hamiltonian will be symmetric.

The reason why the trick works becomes obvious if one looks at the integrand of the discretized integral in the neighborhood of the singularity $p = p'$: i.e.,

$$f(p, p') \equiv [\psi(p') - \psi(p)] \ln \frac{(p - p')^2}{(p + p')^2}. \quad (3.5)$$

There, the function $f(p, p')$ can be extended continuously around $f(p, p) = 0$. Figure 5 demonstrates by way of example that the function is smooth over the whole domain of integration, as opposed to the case when the counterterm is not included. It is well known that integral approximations by Gaussian quadratures are more efficient the smoother the functions are. The basic idea of introducing a counterterm is to account for this fact.

For completeness one should mention that the same method was applied before by Hardekopf and Sucher [21] to relativistic problems (for equal-time quantization), and also that a different method of treating the singularity had been suggested [26], the so-called Galerkin method.

C. Comparison of methods

The results of diagonalizing the Hamiltonian matrix of dimension $N = 128$ are shown in Table I. The numbers in column 1 are obtained solving Eq. (3.2) with a momentum cutoff $\Lambda = 10$. The third one figures the energies won with the convergence generating function $g(p, p')$ as defined by Eq. (3.4). In column 2 we list the results ob-

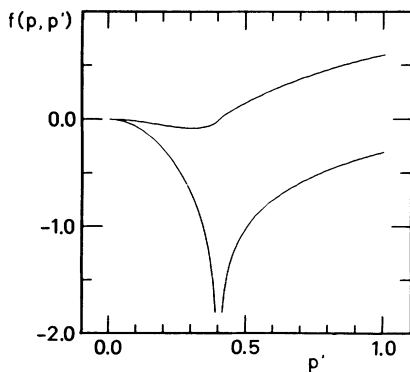


FIG. 5. The quadratic singularity of the integrand, plotted vs p' . Momenta are given in units of the Bohr momentum $p_F = am_r$. The lower curve represents the integrand at $p = 0.4$ without, and the upper curve with the counterterm included, respectively. Note the smooth behavior of the upper as opposed to the singular structure in the lower curve.

tained by a finite interval $D_1 = [0, \Lambda]$, with $\Lambda = 10$ and $g(p, p') \equiv 1$. In all of the cases the integral equation was transformed before discretization by means of the substitution $h(p) = 1/(1+p)$. Thus, the density of abscissa points is increased near the origin. Legendre polynomials in Gaussian quadratures have been used for evaluating the numerical integrations.

The first column should emphasize the insufficiency of solving Eq. (3.2) directly, as opposed to columns 2 and 3 when numerical counterterms are included. In fact, when plotting the eigenvalues as a function of N as done in Fig. 6, one observes an amazing independence of the order of Gaussian quadratures. Already for a 5×5 matrix, the lowest eigenvalues are reproduced quantitatively, and the fact remains when having N significantly increased. We do not know of any other numerical method which combines comparably accuracy with efficiency.

We should mention that the ground-state energy in $\Lambda = \infty$ is exact because of our special choice of the convergence generating function $g(p, p')$. Therefore only the second (or any higher) eigenvalue should be taken as a measure of convergence. The results for $\Lambda = 10$ show how convenient in practice the restriction to a finite domain of integration is. The necessity of choosing large upper bounds is substituted by the slow decrease of the ground-state function. Increasing the cutoff Λ , the computed eigenvalues converge rather fast against the exact values. Setting $\Lambda = 100$ the numbers in the second and third column in Table I become identical (for equal N).

The higher the energy of the (s) states, the more nodes are in the wave functions, and it should be no surprise that more points are needed to reproduce them. This is illustrated in Fig. 7, where it is shown also that the (s) wave functions $\psi_n \propto 1/[(1/n^2) + p^2]^2$ are reproduced most accurately.

Concluding one should state that the Coulomb singularity is present always when working in a momentum

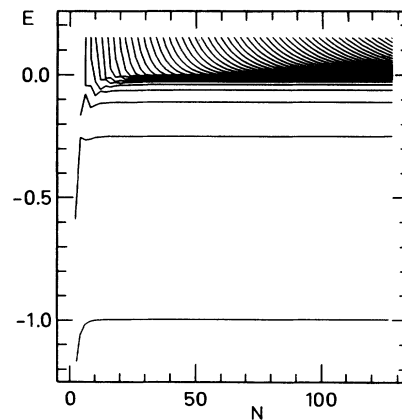


FIG. 6. The eigenvalues of the s states for the Coulomb Schrödinger equation vs the number of integration points $N = 2[2]128$. Calculations including the Coulomb counter term are done for $\Lambda = 10$. Note that fast convergence with N , and that a 10×10 matrix ($N = 10$) suffices to calculate the lowest eigenvalues reliably.

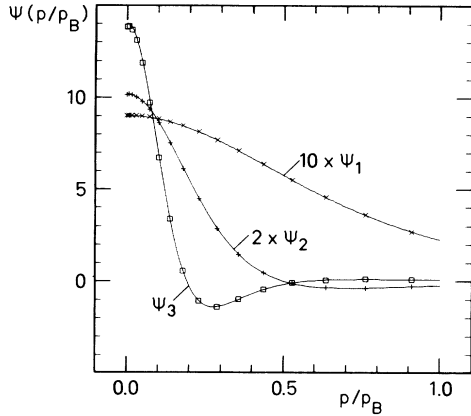


FIG. 7. The analytic s -state wave functions $\psi_n(p)$ are plotted as solid lines vs the absolute value of the momentum p for the lowest nodal numbers $n = 1, 2$, and 3 . They are compared with the eigenfunctions as generated numerically for $\Lambda = 10$, and labeled by (x) , $(+)$, and (\diamond) , correspondingly. Note the excellent agreement, although the number of points (and the matrix dimension) is only $N = 32$. Note also, that the scale of ψ_1 and ψ_2 is compressed by a factor 10 and 2, respectively.

representation. Coulomb counterterms therefore seem to be most important to achieve reasonable convergence at comparatively low numerical resolution.

D. Solving the light-cone Schrödinger equation

The Coulomb singularity is present also in the light-cone Schrödinger equation. When solving Eq. (2.18) numerically, one uses Gaussian quadratures, and therefore has to apply the Coulomb trick again. One adds and subtracts a counterterm from the left-hand side (LHS) of the equation, i.e., $[C_{cc}(x, \mathbf{k}_\perp) - C_{cd}(x, \mathbf{k}_\perp)]\psi(x, \mathbf{k}_\perp)$, whose continuum part is given by

$$C_{cc}(x, \mathbf{k}_\perp) = -\frac{\alpha}{2\pi^2} \times \int_{D_c} dx' d^2\mathbf{k}'_\perp \frac{8m_F^2}{4m_F^2(x-x')^2 + (\mathbf{k}'_\perp - \mathbf{k}_\perp)^2}. \quad (3.6)$$

The discrete part C_{cd} has the same structure, but being discretized and taken at the very same integration points as the discretized version of Eq. (2.18). The Coulomb domain D_c must therefore be the same in both terms in order that they cancel in the continuum limit, but it need not be identical with the domain defined in Eq. (2.15), as long as $D_c \subset D$ and D_c covering the singularity. In what follows we shall use $\Lambda_c = \Lambda$ and

$$D_c: (x-x')^2 + \frac{(\mathbf{k}_\perp - \mathbf{k}'_\perp)^2}{\Lambda_c^2 + 4m_F^2} \leq \bar{R}^2, \quad (3.7)$$

defining a sphere with the dimensionless “radius” \bar{R}

around the point (x, \mathbf{k}_\perp) . In order to satisfy $D_c \subset D$, \bar{R} depends itself on x and \mathbf{k}_\perp^2 : i.e.,

$$\bar{R} = \frac{1}{2} \left[\frac{\Lambda_c^2}{\Lambda_c^2 + 4m_F^2} \right]^{1/2} - \left[(x - \frac{1}{2})^2 + \frac{\mathbf{k}_\perp^2}{\Lambda_c^2 + 4m_F^2} \right]^{1/2}. \quad (3.8)$$

The three-dimensional integral can be evaluated analytically: i.e.,

$$C_{cc}(x, \mathbf{k}_\perp) = -\frac{8\alpha}{\pi} m_F^2 \bar{R}(x, \mathbf{k}_\perp) \left[1 + \frac{4m_F^2}{\Lambda_c^2} \right]^{1/2} \times \ln \left| \frac{\Lambda_c + \sqrt{\Lambda_c^2 + 4m_F^2}}{\Lambda_c - \sqrt{\Lambda_c^2 + 4m_F^2}} \right|. \quad (3.9)$$

More technical details for solving the integral equations are given below. As displayed in Fig. 8, the numerical spectra of the light-cone Schrödinger equation converge rapidly to something like the Bohr spectrum with the increasing number of mesh points. This was not the case without the Coulomb counterterms; in fact, convergence if any was even worse than the one displayed in Fig. 4 for the nonrelativistic equation. The corresponding calculations for varying Λ are compiled in Table II. The extrapolation to $\Lambda \rightarrow \infty$ is done by a Padé approximation. The small but significant deviation of the binding coefficient from the Bohr value 1.0 in the limit $\Lambda \rightarrow \infty$ is no numerical effect but attributed to the fact that the light-cone Schrödinger equation is similar to but not identical with the Coulomb Schrödinger equation. In particular it is not rotationally invariant and therefore the $2s$ and $2p$ states are not completely degenerate (see Fig. 8).

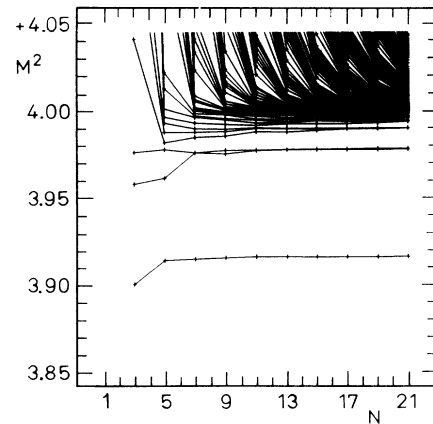


FIG. 8. The invariant mass squared eigenvalues of the light-cone Schrödinger equation vs the number of integrations points N . Note the good convergence with N towards the nonrelativistic values. Calculations are done for $J_z = 0$, $\Lambda = m_F$, and $\alpha = 0.3$. The analytic Coulomb counterterm is included.

TABLE II. The binding coefficient for the light-cone Schrödinger equation. The binding coefficient B_s is given as a function of Λ for the lowest eigenvalue corresponding to the $1s$ state. Masses are in units of m_F . Calculations are done for $\alpha=0.3$ with $N=15$ integration points. The extrapolation to $\Lambda \rightarrow \infty$ was done with the Padé approximation $f(\Lambda)=(c_1+c_2/\Lambda)/(1+c_3/\Lambda)$ using the values $\Lambda=1.0, 3.0$, and 5.0 .

Λ	1.0	2.0	3.0	4.0	5.0	Padé
B_s	0.9355	0.9757	0.9813	0.9827	0.9851	0.9896

IV. SOLVING NUMERICALLY THE TAMM-DANCOFF EQUATION

Dealing with the model of including only one dynamical photon one faces a whole sequence of approximations: DLCQ matrix equation \Rightarrow Tamm-Dancoff equation \Rightarrow light-cone Schrödinger equation \Rightarrow Coulomb Schrödinger equation. All of these approximate treatments, have now been investigated numerically. The solution to the “master equation” (the matrix equation) is given separately [16]. The solutions to the Coulomb and to the light-cone Schrödinger equation is given above. The solution to Tamm-Dancoff equation will be presented below. For all of them hold that the numerical effort is remarkably small when the numerical methods are optimized to the particular problem. A particular aspect of optimization is the inclusion of symmetries.

A. Implementing the symmetries

Not all of the approaches to gauge field theory respect the elementary symmetries of the Lagrangian, by the nature of their construction. The exact Lagrangian symmetries are however not violated by DLCQ or the above model, not even by the *ad hoc* assumptions.

The rotational symmetry. The Lagrangian is invariant under an arbitrary rotation of the coordinate system in the x - y plane, related to an exact quantum number, the projection of the total angular momentum J_z . Introducing the coordinates $(\mathbf{k}_1)_x = k_1 \cos\varphi$ and $(\mathbf{k}_1)_y = k_1 \sin\varphi$, one can Fourier transform the continuum version of the Tamm-Dancoff Eq. (2.14), and in particular the effective potential V_{eff} , according to

$$\frac{1}{2\pi} \int_0^{2\pi} d\varphi e^{-iL_z\varphi} \int_0^{2\pi} d\varphi' e^{+iL'_z\varphi'} \langle x, k_1, \varphi; s_e, s_{\bar{e}} | V_{\text{eff}} | x', k'_1, \varphi'; s'_e, s'_{\bar{e}} \rangle = \langle x, k_1, L_z; s_e, s_{\bar{e}} | \tilde{V}_{\text{eff}} | x', k'_1, L'_z; s'_e, s'_{\bar{e}} \rangle. \quad (4.1)$$

In a way, one replaces the azimuthal angle φ by the projection of the orbital angular momentum $L_z=0, \pm 1, \dots$ as a variable, but neither L_z nor $S_z=s_e+s_{\bar{e}}$ is a good quantum number. The explicit expressions for the matrix elements of \tilde{V}_{eff} are derived straightforwardly from those in Tables VII–IX. For the case $J_z=0$, they are compiled in Table IV. (See also Table III.)

The point symmetries. The Lagrangian is also invariant under the operation of *charge conjugation* \mathcal{C} , *parity* \mathcal{P} , and *time reversal* \mathcal{T} . In the present approach, they are associated with unitary or antiunitary [27] *matrices* U or

V , respectively.

The light-cone Hamiltonian is invariant under charge conjugation. One can thus construct eigenstates of charge conjugation, with eigenvalues $\pi_{\mathcal{C}}=\pm 1$. The creation operators of the electrons b^\dagger , positrons d^\dagger , and photons a^\dagger transform like [28]

$$\begin{aligned} U_{\mathcal{C}} b_s^\dagger(x, \mathbf{k}_1) U_{\mathcal{C}}^{-1} &= d_s^\dagger(x, \mathbf{k}_1), \\ U_{\mathcal{C}} a_\sigma^\dagger(x, \mathbf{k}_1) U_{\mathcal{C}}^{-1} &= -a_\sigma^\dagger(x, \mathbf{k}_1), \\ U_{\mathcal{C}} d_s^\dagger(x, \mathbf{k}_1) U_{\mathcal{C}}^{-1} &= b_s^\dagger(x, \mathbf{k}_1), \end{aligned} \quad (4.2)$$

TABLE III. Spectroscopic notation and discrete symmetries. The relation with $\pi_{\mathcal{H}}=PT=P(-1)^J$ and $\pi_{\mathcal{C}}=C$ is given explicitly for $J_z=0$.

$2S+1L_J$	J^{PC}	$\pi_{\mathcal{H}}$	$\pi_{\mathcal{C}}$	$2S+1L_J$	J^{PC}	$\pi_{\mathcal{H}}$	$\pi_{\mathcal{C}}$
1S_0	0^{-+}	-1	+1	3S_1	1^{--}	+1	-1
3P_0	0^{++}	+1	+1	3D_1	1^{--}	+1	-1
3P_1	1^{++}	-1	+1	3D_2	2^{--}	-1	-1
3P_2	2^{++}	+1	+1	3D_3	3^{--}	+1	-1
1P_1	1^{+-}	-1	-1	1D_2	2^{-+}	-1	+1

where the fermions carry spin $s = \pm \frac{1}{2}$, and the bosons helicity $\sigma = \pm 1$. The P -space wave function reads

$$\Psi_{e\bar{e}}(x, \mathbf{k}_\perp, s_e, s_{\bar{e}}) b_{s_e}^\dagger(x, \mathbf{k}_\perp) d_{s_{\bar{e}}}^\dagger(1-x, -\mathbf{k}_\perp) |0\rangle. \quad (4.3)$$

There are two eigenstates of \mathcal{C} : i.e.,

$$|\pi_{\mathcal{C}} = \pm 1\rangle = \frac{1}{\sqrt{2}} \Psi_{e\bar{e}}(x, \mathbf{k}_\perp, s_e, s_{\bar{e}}) (b_{s_e}^\dagger d_{s_{\bar{e}}}^\dagger \mp b_{s_{\bar{e}}}^\dagger d_{s_e}^\dagger) |0\rangle, \quad (4.4)$$

if the quantum numbers of the electron and the positron differ. When they are the same, the wave function (4.3) is an eigenstate of \mathcal{C} with eigenvalue $\pi_{\mathcal{C}} = -1$.

Neither \mathcal{P} nor \mathcal{T} is an explicit symmetry of the light-cone Hamiltonian, because \mathcal{P} and \mathcal{T} do not leave the $x^+ = 0$ plane invariant. Parity interchanges x^+ and x^- .

But $\exp(-i\pi J_3) \mathcal{P} \mathcal{T}$, for example, or $\exp(-i\pi J_1) \mathcal{P}$ are exact symmetries [5,16,29]. In the sequel, we shall use the combined symmetry $\mathcal{H} \equiv \mathcal{P} \mathcal{T}$, and for having no better word, we call it the *handedness*. Associating with \mathcal{H} the antiunitary matrix $V_{\mathcal{H}} \equiv U_{\mathcal{P}} \otimes V_{\mathcal{T}}$, the parton operators transform according to

$$\begin{aligned} V_{\mathcal{H}} b_s^\dagger(x, \mathbf{k}_\perp) V_{\mathcal{H}}^{-1} &= (-1)^{s-1/2} b_{-s}^\dagger(x, \mathbf{k}_\perp), \\ V_{\mathcal{H}} a_\sigma^\dagger(x, \mathbf{k}_\perp) V_{\mathcal{H}}^{-1} &= -a_{-\sigma}^\dagger(x, \mathbf{k}_\perp), \\ V_{\mathcal{H}} d_s^\dagger(x, \mathbf{k}_\perp) V_{\mathcal{H}}^{-1} &= (-1)^{s+1/2} d_{-s}^\dagger(x, \mathbf{k}_\perp). \end{aligned} \quad (4.5)$$

Note that the handedness just reverts the spins (or helicities) of *all partons*, up to a phase factor which depends on the conventions [27,28]. The eigenfunctions of \mathcal{H} with eigenvalues $\pi_{\mathcal{H}} = \pm 1$ are easily constructed:

TABLE IV. The matrix elements of the effective interaction for $J_z = 0$.

$\frac{\pi}{\alpha} \langle x, k_\perp, J_z, s_1, s_2 \tilde{V}_{\text{eff}}(\omega^*) x' k'_\perp, J_z, s'_1, s'_2 \rangle$	Helicity factors
$m_F^2 \frac{(x'-x)^2}{(1-x')x'(1-x)x} A$	$\delta_{-s_2, s'_2} \delta_{s_2, s'_1} \delta_{s_1, -s'_1}$
$-m_F \frac{1}{x'x} s_1 \left[\frac{1}{k_\perp} B + k_\perp \frac{1-x'}{1-x} A \right]$	$\delta_{s_2, s'_2} \delta_{s_1, s'_2} \delta_{-s_1, s'_1}$
$+m_F \frac{1}{x'x} s_1 \left[\frac{1}{k'_\perp} B + k'_\perp \frac{1-x}{1-x'} A \right]$	$\delta_{s_2, s'_2} \delta_{s_1, -s'_2} \delta_{-s_1, s'_1}$
$+m_F \frac{1}{(1-x')(1-x)} s_1 \left[\frac{1}{k_\perp} B + k_\perp \frac{x'}{x} A \right]$	$\delta_{s_2, -s'_2} \delta_{-s_1, s'_2} \delta_{s_1, s'_1}$
$+m_F \frac{1}{(1-x')(1-x)} s_1 \left[\frac{1}{k'_\perp} B + k'_\perp \frac{x}{x'} A \right]$	$\delta_{s_2, -s'_2} \delta_{s_1, s'_2} \delta_{s_1, s'_1}$
$-A \left[m_F^2 \left[\frac{1}{xx'} + \frac{1}{(1-x)(1-x')} \right] + \frac{k_\perp^2}{x(1-x)} + \frac{k'_\perp{}^2}{x'(1-x')} \right]$	$\delta_{s_2, s'_2} \delta_{s_2, -s'_1} \delta_{s_1, s'_1}$
$-A \frac{1}{xx'(1-x)(1-x')} k_\perp k'_\perp$	$\delta_{s_2, s'_2} \delta_{s_1, s'_2} \delta_{s_1, s'_1}$
$+B \left[\frac{1}{xx'} + \frac{1}{(1-x)(1-x')} \right]$	$\delta_{s_2, s'_2} \delta_{s_2, -s'_1} \delta_{s_1, s'_1}$
$+B \left[\frac{1}{xx'} + \frac{1}{(1-x)(1-x')} \right] \frac{1}{k_\perp k'_\perp} m_F^2$	$\delta_{s_2, s'_2} \delta_{s_1, s'_2} \delta_{s_1, s'_1}$

Abbreviations

$$\begin{aligned} A &= \frac{1}{\sqrt{a^2 - 4k_\perp^2 k'_\perp{}^2}}; \quad B = \frac{1}{2}(1 + aA); \\ a &= -(x-x')^2 \frac{m_F^2}{2} \left[\frac{1}{x'x} + \frac{1}{(1-x')(1-x)} \right] - (k_\perp^2 + k'_\perp{}^2) \\ &\quad + (x-x') \left[\frac{k'_\perp{}^2}{2} \left[\frac{1}{1-x'} - \frac{1}{x'} \right] + \frac{k_\perp^2}{2} \left[\frac{1}{x} - \frac{1}{1-x} \right] \right] \end{aligned}$$

TABLE V. The singlet binding and the hyperfine coefficient for the light-cone Tamm-Dancoff equation as functions of Λ and α . Calculations were done with $N=15$ integration points. For convenience they are extrapolated to $\Lambda \rightarrow \infty$ with a Padé functional $f(\Lambda) = (c_1 + c_2/\Lambda)/(1 + c_3/\Lambda)$ using the values $\Lambda = 1.0, 3.0,$ and 5.0 .

Λ	$\alpha = \frac{3}{10}$			$\Lambda \frac{1}{3\alpha}$	$\alpha = \frac{1}{137}$		
	B_s	B_t	C_{hf}		B_s	B_t	C_{hf}
1.0	1.0486	0.9999	0.1354	1.0	0.9328	0.9328	0.1028
2.0	1.1797	1.0752	0.2903	2.0	0.9872	0.9871	0.1970
3.0	1.2344	1.0948	0.3876	3.0	0.9955	0.9955	0.2393
4.0	1.2681	1.1043	0.4550	4.0	0.9980	0.9979	0.2617
5.0	1.2927	1.1105	0.5062	5.0	0.9990	0.9989	0.2753
6.0	1.3122	1.1151	0.5475	6.0	0.9996	0.9996	0.2844
7.0	1.3285	1.1189	0.5822	7.0	1.0001	1.0000	0.2908
8.0	1.3426	1.1222	0.6122	8.0	1.0005	1.0004	0.2956
9.0	1.3552	1.1252	0.6389	9.0	1.0008	1.0008	0.2993
10.0	1.3666	1.1279	0.6630	10.0	1.0012	1.0012	0.3022
Padé	1.4046	1.1323	0.8356	Padé	1.0029	1.0028	0.3371

$$\begin{aligned}
|\pi_{\mathcal{H}} = \pm 1\rangle &= \frac{1}{\sqrt{2}} \Psi_{e\bar{e}}(x, \mathbf{k}_\perp, s_e, s_{\bar{e}}) b_{+s_e}^\dagger(x, \mathbf{k}_\perp) d_{s_{\bar{e}}}^\dagger(1-x, -\mathbf{k}_\perp) |0\rangle \\
&\pm \frac{(-1)^{s_e + s_{\bar{e}}}}{\sqrt{2}} \Psi_{e\bar{e}}^*(x, \mathbf{k}_\perp, s_e, s_{\bar{e}}) b_{-s_e}^\dagger(x, \mathbf{k}_\perp) d_{-s_{\bar{e}}}^\dagger(1-x, -\mathbf{k}_\perp) |0\rangle
\end{aligned} \tag{4.6}$$

for the case of the P -space wave function.

Relation to spectroscopic notation. We shall discuss the results in terms of the spectroscopic notation, using J , L , and S , the quantum numbers of total, orbital, and spin angular momentum, respectively. Adopting a particular time-reversal convention [30] $V_T |J, J_z\rangle = (-1)^{J-J_z} |J, -J_z\rangle$, one can relate them to the above quantum numbers. A compilation for the first few cases is given in Table III for $J_z = 0$. In the sequel the integral

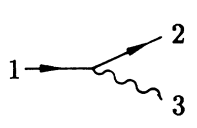
equation is solved only for the $J_z = 0$ subspace, with special emphasis to the ground and the first excited state, i.e., to parapositronium (1^1S_0) and to orthopositronium (1^3S_1), respectively.

Using the rotational symmetry the dimensionality of the problem reduces from 3 to 2, i.e., one saves a *factor* 10–30 in the dimension of the Hamiltonian, depending on the number of integration points. The point symmetries provide another factor of 4. Since the computa-

TABLE VI. The dependence of binding energies on the cutoff Λ . Calculations were done for the light-cone Tamm-Dancoff equation with the modified interaction V_{mod} using 41 integration points in μ and 11 points in $\cos\theta$. The nonrelativistic (NR) values are added for convenience. Note the improved convergence as compared to Table V.

$\Lambda \frac{1}{6\alpha}$	$\alpha = \frac{3}{10}$			$\Lambda \frac{1}{6\alpha}$	$\alpha = \frac{1}{137}$		
	B_s	B_t	C_{hf}		B_s	B_t	C_{hf}
1.0	1.0816	1.0047	0.2135	1.0	0.987 645	0.987 603	0.1972
2.0	1.1239	1.0157	0.3005	2.0	0.998 186	0.998 130	0.2622
3.0	1.1377	1.0171	0.3351	3.0	0.999 437	0.999 376	0.2853
4.0	1.1449	1.0174	0.3539	4.0	0.999 647	0.999 584	0.2968
5.0	1.1494	1.0176	0.3661	5.0	0.999 881	0.999 816	0.3040
6.0	1.1526	1.0177	0.3746	6.0	0.999 936	0.999 871	0.3086
7.0	1.1549	1.0178	0.3810	7.0	0.999 966	0.999 899	0.3119
8.0	1.1568	1.0178	0.3861	8.0	0.999 983	0.999 916	0.3143
9.0	1.1583	1.0178	0.3902	9.0	0.999 994	0.999 926	0.3164
10.0	1.1595	1.0178	0.3936	10.0	1.000 001	0.999 933	0.3178
NR	1.1181	0.9981	0.3333	NR	1.000 070	0.999 999	0.3333

TABLE VII. The matrix elements of the vertex interaction V . The coupling constant α is hidden in $\beta=8\pi\alpha/(P^+\Omega)$. In the continuum limit one replaces sums by integrals and β by $\tilde{\beta}\equiv C_L\beta=\alpha/2\pi^2$. The transverse polarization vector is defined as $\epsilon_\perp(\lambda)=(-\lambda\hat{x}-i\hat{y})/\sqrt{2}$.

Graph	Matrix Element	= Momentum \times	Helicity
	$V_{q \to qg}(1; 2, 3)$	$\sqrt{\beta} \frac{1}{\sqrt{x_3}} m_F \left[\frac{1}{x_2} - \frac{1}{x_1} \right]$ $+\sqrt{2\beta} \frac{1}{\sqrt{x_3}} \vec{\epsilon}_\perp(\lambda_3) \cdot \left[\left(\frac{\vec{k}_\perp}{x} \right)_3 - \left(\frac{\vec{k}_\perp}{x} \right)_2 \right]$ $+\sqrt{2\beta} \frac{1}{\sqrt{x_3}} \vec{\epsilon}_\perp(\lambda_3) \cdot \left[\left(\frac{\vec{k}_\perp}{x} \right)_3 - \left(\frac{\vec{k}_\perp}{x} \right)_1 \right]$	$\delta_{-\lambda_1}^{\lambda_2} \delta_{\lambda_1}^{\lambda_3}$ $\delta_{+\lambda_1}^{\lambda_2} \delta_{\lambda_1}^{\lambda_3}$ $\delta_{+\lambda_1}^{\lambda_2} \delta_{-\lambda_1}^{\lambda_3}$
$V = \sum_{q_1, q_2, q_3} (b_1^\dagger b_2 a_3 - d_1^\dagger d_2 a_3) V_{q \to qg}(1; 2, 3)$ $+ \sum_{q_1, q_2, q_3} (a_3^\dagger b_2^\dagger b_1 - a_3^\dagger d_2^\dagger d_1) V_{q \to qg}^*(1; 2, 3)$			

tional time for matrix diagonalization increases like N^3 with the matrix dimension N , one reduces the effort by a factor $\sim 10^5$ without any loss of accuracy.

B. The spectrum and the wave function

Instead of x, k_\perp (and φ) one preferably uses [20] kind of spherical momentum coordinates μ, θ as defined by

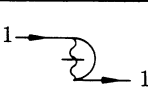
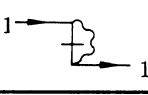
$$k_\perp = \mu \sin\theta \quad \text{and} \quad x = \frac{1}{2} + \frac{\mu}{2} \frac{\cos\theta}{\sqrt{m_F^2 + \mu^2}}. \quad (4.7)$$

Since the invariant mass is $(m_F^2 + k_\perp^2)/x(1-x) = 4m_F^2 + 4\mu^2$, μ can be interpreted as an off-shell mass, or as a generalization of the nonrelativistic momentum $|\mathbf{k}|$. Fock-space regularization translates then into $\mu \leq \Lambda/2$, see also Eqs. (2.15) and (2.19). Since the integrals are

evaluated by Gaussian quadratures, μ and $\cos\theta$ are to be taken at discrete longitudinal and angular integration points, respectively. If not mentioned otherwise, the same number N is taken in either direction.

Which Coulomb counterterm should be used? One might conjecture that the residue at the Coulomb singularity depends sufficiently weakly on the off-shell momenta in order to use the analytical expression, Eq. (3.9). In practice, however, this counterterm turns out insufficient, as shown in Fig. 9. Although one recognizes the singlet and triplet are correct by order of magnitude, one observes an unpleasant sensitivity to N . Particularly in view of the high numerical precision required, one has to resort to the full counterterm. Its continuum part is defined by

TABLE VIII. The matrix elements of the contraction terms C . The coupling constant α is hidden in $\beta=8\pi\alpha/(P^+\Omega)$. In the continuum limit one replaces sums by integrals and β by $\tilde{\beta}\equiv C_L\beta=\alpha/2\pi^2$.

Type	Graph	Matrix Element
$C(q_1)$		$C^{(g)}(q_1) = \beta \frac{1}{x_1} \sum_{y, \vec{k}_\perp} \frac{2}{y^3}$
		$C^{(q)}(q_1) = \beta \frac{1}{x_1} \sum_{y, \vec{k}_\perp} \frac{1}{y}$
$C = \sum_{q_1} (b_1^\dagger b_1 + d_1^\dagger d_1) C(q_1)$		

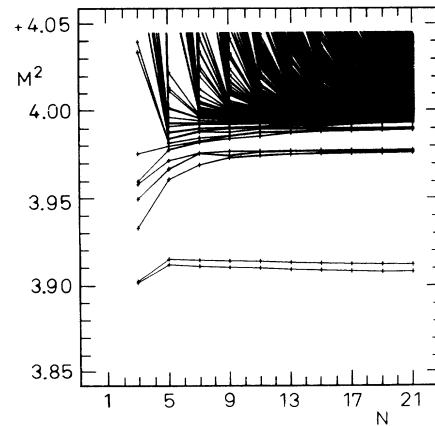


FIG. 9. The invariant mass squared eigenvalues of the Tamm-Dancoff equation vs the number of integration points N . Note the reasonable convergence with N , and the appearance of the hyperfine splitting. Calculations are done for $J_z=0$, $\Lambda=m_F$, and $\alpha=0.3$ and with the analytical Coulomb counterterm for the light-cone Schrödinger equation.

$$C_{cc}(x, k_{\perp}) = \int_{D_c} dx' d^2 k'_{\perp} \langle x, k_{\perp}, L_z; s_e, s_{\bar{e}} | \bar{V}_{\text{eff}} | x', k'_{\perp}, L'_z; s'_e, s'_{\bar{e}} \rangle. \quad (4.8)$$

Unfortunately, the advantage of an analytical expression fades away. Two of the three integrations can be done easily by analytical quadratures, but the third one has to be done numerically with sufficiently high resolution.

The so-obtained spectrum is given in Fig. 10. One recognizes the appearance of the singlet and triplet state, as well as the higher parts of the spectrum at roughly the correct values, and that they approach a stable limit as functions of the resolution N . The comparatively slow convergence of the higher states is no surprise, and was observed already in the much more trivial case of Fig. 6: Although the wave functions in momentum space are localized also at $x \approx \frac{1}{2}$ and $k_{\perp} \approx 0$, they have more nodal structures. Consequently, one needs more integration

points to account for them.

One should emphasize that the numerical methods are obviously rather efficient. For example, only a 25×25 matrix (for $N=5$) is needed to render the singlet and the triplet state reasonably stable as functions of N . This corresponds to only two transverse-momentum points. One should emphasize also that these calculations add evidence to the requirement that the longitudinal and transverse continuum limit of DLCQ exists *at all*.

How sensitive are the results to the value of the cutoff? Do the numerical results converge with Λ , and do they agree with the analytical predictions? These questions cannot be investigated at the comparatively rough scale of a figure such as Fig. 10. The binding coefficients for

TABLE IX. The matrix elements of the seagull interaction S . The coupling constant α is hidden in $\beta = 8\pi\alpha/(P^+\Omega)$. In the continuum limit one replaces sums by integrals and β by $\tilde{\beta} \equiv C_L\beta = \alpha/2\pi^2$.

Type	Graph	Matrix Element	Momentum \times Helicity Factor
S_1		$S_{qq \rightarrow qq}(1, 2; 3, 4)$	$-\beta \frac{1}{(x_1 - x_3)^2} \delta_{\lambda_1}^{\lambda_3} \delta_{\lambda_2}^{\lambda_4}$
S_3		$S_{qq}^{(s)} \rightarrow qq(1, 2; 3, 4)$	$\beta \frac{2}{(x_1 - x_3)^2} \delta_{\lambda_1}^{\lambda_3} \delta_{\lambda_2}^{\lambda_4}$
		$S_{qq}^{(a)} \rightarrow qq(1, 2; 3, 4)$	$-\beta \frac{2}{(x_1 + x_2)^2} \delta_{-\lambda_1}^{\lambda_2} \delta_{-\lambda_3}^{\lambda_4}$
S_5		$S_{qg}^{(s)} \rightarrow qg(1, 2; 3, 4)$	$\beta \frac{1}{x_1 - x_4} \frac{1}{\sqrt{x_2 x_4}} \delta_{\lambda_1}^{\lambda_3} \delta_{\lambda_2}^{\lambda_4} \delta_{\lambda_1}^{\lambda_2}$
		$S_{qg}^{(a)} \rightarrow qg(1, 2; 3, 4)$	$\beta \frac{1}{x_1 + x_2} \frac{1}{\sqrt{x_2 x_4}} \delta_{\lambda_1}^{\lambda_3} \delta_{\lambda_2}^{\lambda_4} \delta_{-\lambda_1}^{\lambda_2}$
S_7		$S_{qg} \rightarrow gq(1, 2; 3, 4)$	$\beta \frac{1}{x_1 - x_3} \frac{1}{\sqrt{x_2 x_4}} \delta_{-\lambda_1}^{\lambda_2} \delta_{-\lambda_3}^{\lambda_4} \delta_{\lambda_1}^{\lambda_3}$
$S = \sum_{q_1, q_2, q_3, q_4} (b_1^\dagger b_2^\dagger b_3 b_4 + b_4^\dagger b_3^\dagger b_2 b_1) S_1(1, 2; 3, 4)$ $+ \sum_{q_1, q_2, q_3, q_4} b_1^\dagger d_2^\dagger b_3 d_4 S_3(1, 2; 3, 4)$ $+ \sum_{q_1, q_2, q_3, q_4} (b_1^\dagger a_2^\dagger b_3 a_4 + d_1^\dagger a_2^\dagger d_3 a_4) S_5(1, 2; 3, 4)$ $+ \sum_{q_1, q_2, q_3, q_4} (b_1^\dagger d_2^\dagger a_3 a_4 + a_4^\dagger a_3^\dagger d_2 b_1) S_7(1, 2; 3, 4)$			

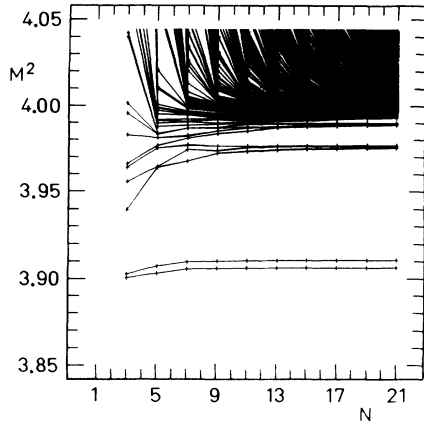


FIG. 10. The invariant mass squared eigenvalues of the Tamm-Dancoff equation vs the number of integration points N . Note the good convergence with N , and the appearance of the hyperfine splitting. Calculations are done for $J_z=0$, $\Lambda=m_F$, and $\alpha=0.3$. The numerically integrated Coulomb counterterm for the Tamm-Dancoff equation is included.

the singlet and triplet state are therefore tabulated in Table V for ten values of Λ and two values of α , together with the hyperfine coefficient.

For $\alpha=\frac{1}{137}$, one should emphasize first that the calculated mass square deviates extremely little from the free value $4m_F$. A reliable extraction of the data in Table V requires therefore a numerical accuracy with ten significant figures. The fact that the calculations do not become numerically unstable as functions of Λ is taken as a valuable indicator of the overall numerical accuracy of the codes. Second, one observes with these numbers a similar behavior as for the nonrelativistic case in Table I. One needs a couple of Bohr momenta, i.e., $\Lambda=Cam_F$, before the numbers begin to converge. With increasing Λ however, the typical relativistic effects become important. One cannot separate these ones from the others, and one observes a very small but significant dependence on the increasing cutoff. Nevertheless, the calculated hyperfine shift is reasonably in between the Fermi and the Bodwin values.

For the very large value of the coupling constant $\alpha=\frac{3}{10}$, the numbers in Table V agree with the analytical predictions by order of magnitude—but not much more. They agree less than, for example, the recent results of Koniuk and co-workers [31,32] for the very same model but in *equal usual time* quantization. The dependence of the results on Λ is much more accentuated than for the small value of α . The present calculation *overbinds* positronium, since one gets numerically $B_s \sim 1.40$ instead of the predicted $B_s=1.118$, and similarly for the triplet. Also the hyperfine shift is larger than predicted. In order to guide the eye, the table includes a Padé extrapolation, which however is a meaningful concept only when the results vary like an inverse power of the cutoff.

What is the functional dependence on Λ ? At first, it might look as if the binding coefficients vary logarithmic-

ally with the cutoff, i.e., like $\sqrt{\ln\Lambda}$. But the results are also consistent with an inverse power law, as found by detailed analysis of the numbers. The problem is related to the structure of the relativistic interaction, Eq. (2.16). At fixed values of x, x' , and \mathbf{k}_\perp , both the numerator and the denominator are governed by $\mathbf{k}_\perp'^2$, such that the interaction tends to a constant for sufficiently large values of $\mathbf{k}_\perp'^2$. A logarithmic behavior could thus be understood if the wave function behaves asymptotically like $\text{const}\mu^\kappa$ with a slope parameter $\kappa=-2$. In Fig. 11 the wave functions are displayed for both values of α . Remarkably, the numerical results for the small coupling constant follow almost identically the analytic nonrelativistic solution, over more than six orders of magnitude. The slope parameter κ agrees with the nonrelativistic value $\kappa=-4$ to within three relevant figures. Note the contrast with the coupling case. The relativistic effects become obviously more important since the slope is close to $\kappa=-2.5$. A logarithmic dependence of the eigenvalues is therefore less likely, although one cannot exclude positively an even slower decay at momenta even higher than the large cutoff $\Lambda=10m_F$. The latter is large by all standards, the minimum of the longitudinal-momentum fraction for this cutoff is as small as $x_{\min} \sim m_F^2/\Lambda^2 \sim 0.01$, see Eq. (4.7).

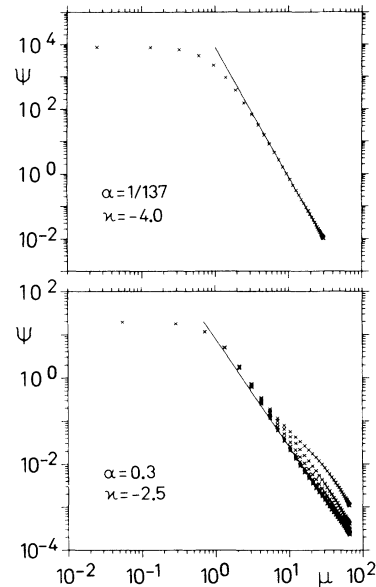


FIG. 11. The leading component of the singlet wave function on the Gaussian mesh, i.e., $\Psi_{\uparrow 1}(\mu_i, \cos\theta_j)$, is plotted for all integration points $i=1, \dots, 41$ vs the off-shell mass μ in units of the Bohr momentum $p_B=\frac{1}{2}m_F\alpha$. The curves for $j=1, \dots, 12$ are plotted on top of each other to show a possible deviation from rotational symmetry. The upper plot shows the results for the small coupling constant $\alpha=1/137$ with a cutoff $\Lambda=30am_F$. The straight line corresponds to $\text{const}\mu^\kappa$ and has the slope $\kappa=-4$. The lower plot shows the results for the large coupling constant $\alpha=0.3$ with a cutoff $\Lambda=10m_F$. The line has the slope $\kappa=-\frac{5}{2}$.

V. DISCUSSION AND IMPROVEMENTS

On the one hand, the numerical results are not really discouraging. For the small value of the coupling constant, in fact, they are quite satisfactory. Even for the large coupling constant $\alpha=0.3$ and the very large cutoff $\Lambda=10m_F$ the calculations overestimate the binding energy only by a few percent. On the other hand, their dependence on the cutoff particularly at strong coupling is intriguing. What is the origin, and how could it be removed? Unfortunately, the kernel of the integral equation in light-cone variables is so complicated that we have been unable to work out the explicit functional dependence of the solutions on Λ . Perhaps, this would be possible in perturbative series, but their combination with bound-state calculations is highly nontrivial [12]. Therefore, in the present context, one cannot apply procedures such as the one proposed by Kinoshita and Lepage [33]. They propose to introduce additional classes of operators subject to vanish in the limit $\Lambda \rightarrow \infty$, and to tailor them at any finite value of Λ such that they cancel an explicit dependence on Λ sufficiently well.

One of the difficulties in interpreting this work is that the peculiarities of light-cone variables and the model aspects are so strong interwoven. We only know with certainty that we have not solved the model formulated in Sec. II, i.e., the model with strictly one dynamical photon. The model with strictly one photon would require to set the ‘‘starting point energy’’ ω equal, or at least approximately equal, to the eigenvalue $\omega \sim (4-\alpha^2)m_F^2$. Like before [6,7,20,31], this was given up because of an essential and untractable singularity $(\omega^*-\omega)/|x-x'|\mathcal{D}$ in the kernel. This singularity vanishes when requiring *ad hoc* $\omega=\omega^*$. But taken at face value, this assumption is horrible. One replaces a *number* by a *function*. That the same assumption gives the usual Coulomb singularity in the nonrelativistic approximation is a welcome byproduct, but despite all these advantages, one loses track of the physical model, unfortunately. What is the physical model, and how could it be improved? Can it be improved at all?

In order to make progress one should generalize the model to include two or more dynamical photons, and then look back on the one-photon case to see perhaps the difference. As it turns out, this is possible, at least conceptually by means of the projector technique introduced in Sec. II. The full problem with arbitrarily many photons can be projected on $e\bar{e}$ space, leading again to an effective Hamiltonian. Unfortunately, the complete, particularly the numerical treatment exceeds the aim and the length of the present work and will be given in forthcoming work. The following outline might however put the present work into the right perspective.

A. The effective Hamiltonian for many photons

The definition of projectors Q_n as introduced in Sec. II is easily generalized to Fock states with n photons, $n=0,1,\dots,N$. The projector technique can then be generalized to many photons, exploiting the fact that the Hamiltonian block matrix $H_{nn'}$ has a pentadiagonal block

structure. This has not been done so far, and is based on the observation that the light-cone Hamiltonian [9,10] cannot change the parton number by more than two. Consequently, the block matrices $H_{nn'}$ vanish identically for $|n-n'|>2$. To remind us of the fact that the vertex interactions change the parton number always by 1 and the fork interactions always by 2, we shall choose the notation $V_{n,n+1} \equiv H_{n,n+1}$ and $F_{n,n+2} \equiv H_{n,n+2}$. As an explicit example, consider the block matrix equation for 3 photons:

$$\begin{pmatrix} H_{00}-\omega & V_{01} & F_{02} & 0 \\ V_{10} & H_{11}-\omega & V_{12} & F_{13} \\ F_{20} & V_{21} & \hat{H}_{22}-\omega & \tilde{V}_{23} \\ 0 & F_{31} & \tilde{V}_{32} & \tilde{H}_{33}-\omega \end{pmatrix} \begin{pmatrix} |\psi\rangle_0 \\ |\psi\rangle_1 \\ |\psi\rangle_2 \\ |\psi\rangle_3 \end{pmatrix} = 0, \quad (5.1)$$

where we have set $\tilde{H}_{33} \equiv H_{33}$, $\tilde{V}_{32} \equiv V_{32}$, and $\hat{H}_{22} \equiv H_{22}$. Consider Eq. (5.1) as a set of coupled linear equations. In analogy with Eq. (2.3), substitute in a first step $|\psi\rangle_3 = (\omega - \tilde{H}_{33})^{-1} \tilde{V}_{32} |\psi\rangle_2 + (\omega - \tilde{H}_{33})^{-1} F_{31} |\psi\rangle_1$. This is a special version of the general reduction scheme

$$|\psi\rangle_n = \frac{1}{\omega - \tilde{H}_{n,n}} \tilde{V}_{n,n-1} |\psi\rangle_{n-1} + \frac{1}{\omega - \tilde{H}_{n,n}} F_{n,n-2} |\psi\rangle_{n-2},$$

with

$$\begin{aligned} \tilde{V}_{n,n+1} &= V_{n,n+1} + F_{n,n+2} \frac{1}{\omega - \tilde{H}_{n+2,n+2}} \tilde{V}_{n+2,n+1}, \\ \tilde{H}_{n,n} &= H_{n,n} + \tilde{V}_{n,n+1} \frac{1}{\omega - \tilde{H}_{n+1,n+1}} \tilde{V}_{n+1,n} \\ &\quad + F_{n,n+2} \frac{1}{\omega - \tilde{H}_{n+2,n+2}} F_{n+2,n}, \\ \hat{H}_{n,n} &= H_{n,n} + F_{n,n+2} \frac{1}{\omega - \tilde{H}_{n+2,n+2}} F_{n+2,n}. \end{aligned} \quad (5.2)$$

After one step, one gets thus

$$\begin{pmatrix} H_{00}-\omega & V_{01} & F_{02} \\ V_{10} & \hat{H}_{11}-\omega & \tilde{V}_{12} \\ F_{20} & \tilde{V}_{21} & \tilde{H}_{22}-\omega \end{pmatrix} \begin{pmatrix} |\psi\rangle_0 \\ |\psi\rangle_1 \\ |\psi\rangle_2 \end{pmatrix} = 0. \quad (5.3)$$

Repeating the procedure one arrives sequentially at

$$\begin{pmatrix} \hat{H}_{00}-\omega & \tilde{V}_{01} \\ \tilde{V}_{10} & \tilde{H}_{11}-\omega \end{pmatrix} \begin{pmatrix} |\psi\rangle_0 \\ |\psi\rangle_1 \end{pmatrix} = 0 \quad (5.4)$$

and

$$\tilde{H}_{00}|\psi\rangle_0 = \omega|\psi\rangle_0.$$

Note that Eqs. (5.4) and (5.3) are identical with Eq. (5.1).

$$H_{\text{eff}}(\omega) = H_{00} + V_{01} \frac{1}{\omega - H_{11} - V_{12} \frac{1}{\omega - H_{22} - V_{23} \frac{1}{\omega - H_{33}} V_{32}} V_{21}} V_{10}. \quad (5.5)$$

Obviously, a continued fraction expansion wants to develop, very similar to formal resummations of perturbative series to all orders [34]. For an arbitrary photon number N , the expansion comes to an end whenever one hits the combination $\omega - H_{NN}$ in the denominator.

One should emphasize that the reduction scheme (5.2) holds also for the general case when including in addition any number of $e\bar{e}$ pairs: the light-cone Hamiltonian is pentadiagonal in the parton number. Equations (5.2)–(5.4) are therefore another and equivalent way of writing down the Bethe-Salpeter equation on the light cone. In principle, a similar reduction scheme could also be derived for the usual equal-time variables, but due to the typical vacuum fluctuation terms, the matrix would have nine block diagonals. The reduction scheme would be correspondingly more complicated and has not been worked out so far.

B. Interpreting the *ad hoc* assumption and the model

Let us now assume to work in a model with two dynamical fermions ($e\bar{e}$), arbitrarily many photons $N \rightarrow \infty$, but no instantaneous fermions interactions at all. By definition, all fork interactions are then absent. The Hamiltonian block matrix is tridiagonal, and the effective interaction has the structure of a “simple” continued fraction, in analogy with Eq. (5.5), which is written as

$$H_{\text{eff}}(\omega) = H_{00} + V_{01} \frac{1}{\omega - H_{11} - W_{11}(\omega)} V_{10}. \quad (5.6)$$

The definition of the iterated vertex interaction $W_{11}(\omega)$ is obvious from a comparison with Eq. (5.5). Combining it with the instantaneous photon interactions hidden in H_{11} into an effective interaction $U_{\text{eff}}(\omega)$ in the $e\bar{e}\gamma$ space, one rewrites Eq. (5.6) identically as

$$H_{\text{eff}}(\omega) = H_{00} + V_{01} \frac{1}{\omega - M_{e\bar{e}\gamma}^2 - U_{\text{eff}}(\omega)} V_{10}. \quad (5.7)$$

When comparing this with Eq. (2.4), one realizes that the higher-photon spaces generate an effective interaction also in $e\bar{e}\gamma$ space. When one replaces the associated resolvent according to

$$\frac{1}{\omega - M_{e\bar{e}\gamma}^2 - U_{\text{eff}}(\omega)} \simeq \frac{1}{\omega^* - M_{e\bar{e}\gamma}^2}, \quad (5.8)$$

In fact, Eqs. (5.1)–(5.4) are identical with Eq. (2.1) for an arbitrary N , as can be shown easily by induction.

The general structure of the effective interaction $H_{\text{eff}} \equiv \tilde{H}_{00}$ is more transparent when omitting the fork matrices F , momentarily. For $N=3$ one gets

one substitutes the sum of kinetic and interaction operators ω^* and $U_{\text{eff}}(\omega)$, respectively, by the eigenvalue, i.e.,

$$\omega^* + U_{\text{eff}}(\omega) \simeq \omega^* + \langle U_{\text{eff}}(\omega) \rangle \simeq \omega. \quad (5.9)$$

Contrary to Eq. (2.7) this is at least plausible, and can be interpreted as resumming the photons to all orders. The incomprehensive *ad hoc* substitution $\omega \Rightarrow \omega^*$ combined with the one-photon model leads to the same final equation only formally.

But despite its plausibility, the so-generated effective interaction seems to be bothered with the fact that the resulting eigenvalues depend on Λ too strongly. The problem can be traced to the $\uparrow\downarrow$ matrix element given in Eq. (2.16), i.e., to that part of it which behaves like

$$V_{\text{eff,con}} = -\frac{\alpha}{2\pi^2} \frac{1}{\mathcal{D}} \left[\frac{\mathbf{k}_1^2}{x(1-x)} + \frac{\mathbf{k}'_1^2}{x'(1-x')} \right]. \quad (5.10)$$

For sufficiently large transverse momenta, e.g., for $k'_1 \gg m_F$ and $k_1 \gg k'_1$ with fixed longitudinal momenta ($x \sim x' \sim \frac{1}{2}$), $V_{\text{eff,con}}$ tends to $-2\alpha/\pi^2$, corresponding to a delta function in configuration space. The larger the cutoff becomes the more of this term is picked up by the wave function. How could one eventually account for this aspect?

One way of avoiding the above asymptotic behavior of the effective interaction is to change it by hand. One could substitute the energy denominator in Eq. (2.13) like $\mathcal{D} \rightarrow \mathcal{D} + \mathcal{D}^2/m_F^2$, i.e.,

$$V_{\text{eff}} \rightarrow V_{\text{mod}} = V_{\text{eff}} \frac{\mathcal{D}}{\mathcal{D} + \mathcal{D}^2/m_F^2}. \quad (5.11)$$

In the vicinity of the Coulomb singularity ($\mathcal{D} \sim 0$), i.e., for small momentum transfer, or correspondingly for large distances, the approximate effective interaction would practically coincide with V_{eff} . Only for relativistic momentum exchanges, or correspondingly for the very small distances, the approximate interaction would differ substantially. But such a procedure is not really satisfactory and we shall pursue another approach in the sequel.

C. Towards a simplified model

One should emphasize that nothing has been solved when writing down an expansion scheme such as in Eqs. (5.2)–(5.4). The only advantage is to see more clearly

certain structures, which we want to develop when the infinite perturbative series are resummed to all orders. The scheme is however particularly suited for a matrix approach such as DLQC, since the “denominators” are the inverses of finite-dimensional matrices. In principle, an expression such as Eq. (5.5) is thus well defined.

Consider the effective interaction in Q -space, as it appears in the denominator of Eq. (5.6). It connects the $e\bar{e}\gamma$ states among each other by finite matrix elements, which for simplicity will be represented graphically, below. The instantaneous interactions contained in H_{11} have already been illustrated in Fig. 5. Some of the iterated vertex interactions W_{11} are given in Fig. 12. They arise due to the scattering into the next higher, $e\bar{e}\gamma\gamma$ space. In principle, the Q -space matrix is therefore nondiagonal. Constructions such as Eq. (5.9) must be interpreted as a diagonalization by brute force. In another approximation scheme, one expands the Q -space resolvent into a series. Restricting to the first nontrivial order, this generates matrix elements in P -space such as those in Fig. 13. Graphs such as 13(a) or 13(b) are directly related to graph 12(a): the Q -space photon plays the role of a spectator. Opposed to this, the photon is a participant in graph 13(c) related to graph 12(b), since it is absorbed and reemitted in Q -space. Graphs such as 13(d) originate from the instantaneous fermion interaction in Q -space, while a graph such as 13(e) is generated by the iterated fork interaction $F_{02}(\omega - H_{22})^{-1}F_{20}$ in Eq. (5.2). All of them have “two photons in flight.” Finally, graph 13(f) referring to the first iteration of the effective interaction in P -space is added to be complete in the terms of order α^2 .

As will be shown elsewhere [35] for the on-shell scattering amplitude, each individual graph in Fig. 13 diverges logarithmically due to the k_1 integration. Particularly, the logarithmic divergence in the partial scattering amplitude corresponding to graph 13(f) is caused by the term corresponding to $V_{\text{eff,con}}$, Eq. (5.10). But when all terms of second order are summed up consistently, i.e., when summing graphs 13(c)–13(f) in all time orderings and in Feynman gauge, the logarithmic singularities *cancel each other*. This result had to be expected since the second-order Feynman amplitude for $e\bar{e}$ scattering has no logarithmic divergencies. Nevertheless, the result is important since a complete analysis of the scattering amplitude up to second order had not been given thus far in light-cone coordinates, particularly not for a Hamiltonian approach, and allows us to propose the following procedure.

To account for retardation effects in an approximate way, we propose to simply omit the worrisome piece, and

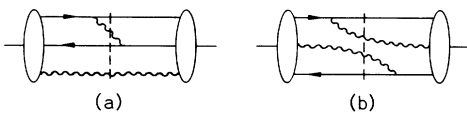


FIG. 12. The Q -space matrix elements generated by the iterated vertex interaction W_{11} are given in diagrammatical form, see discussion in the text.

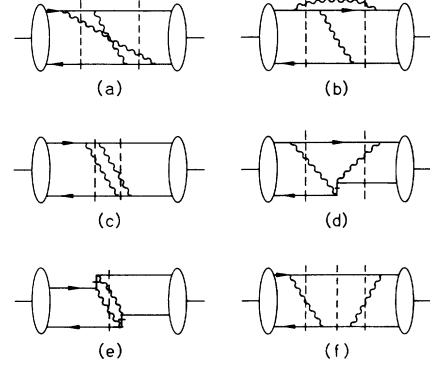


FIG. 13. The P -space matrix elements in an expansion of the Q -space resolvent are given in diagrammatical form for the graphs of order α^2 .

to replace the effective interaction by the modified effective interaction according to

$$V_{\text{eff}} \rightarrow V_{\text{mod}} = V_{\text{eff}} - V_{\text{eff,con}} \delta_{s_1, -s_2}, \quad (5.12)$$

with $V_{\text{eff,con}}$ given by Eq. (5.10). The corresponding numerical values are presented in Table VI. As expected, they differ only little from Table V for the small coupling constant; in fact, they agree even better with the nonrelativistic predictions. We have verified that the extrapolation of the hyperfine coefficient to $\Lambda \rightarrow \infty$ either by a fit or by a Padé functional yields the value 0.331. For the strong-coupling case, however, the results depend much less on Λ , and are in reasonable agreement with prediction. Also the wave function looks reasonable. At sufficiently large momenta, the slope is in between the values $\kappa = -4$ and $\kappa = -2.5$, as was displayed in Fig. 11.

Apart from being very simple, the procedure can be generalized to higher orders of perturbation theory. For example, when formulating the interaction perturbatively in the next higher order ($\sim \alpha^2$), including all graphs as displayed in Figs. 13(a)–13(e), one includes first $V_{\text{eff,con}}$ again and subtracts the piece which in order α^2 tends to a constant. More details will be given in Ref. [35]. The procedure is also applicable in an explicit matrix approach: One adds the corresponding counterterm in the last sector of the effective interaction which is explicitly included. Finally, one should emphasize that the present approach produces a wave function *at all* for an interaction which generates the correct hyperfine splitting; non-relativistically, for example, a solution of a Schrödinger equation including a Serber-Uhling term would not be stable.

D. Application to quantum chromodynamics

In principle one could apply the same model also to quantum chromodynamics. Including only one pair of quark ($q\bar{q}$), arbitrarily many gluons g , omitting *ad hoc* all instantaneous fermion interactions, and replacing the propagator in the manner of Eq. (5.8), one would end up with the same formal equations, except that the coupling constant α would have to be replaced by $\frac{4}{3}\alpha$. The factor

$\frac{4}{3}$ arises by the summation over the colors $n_c = 1, 2, 3$, and would have to be replaced by $(n_c^2 - 1)/2n_c$ for general non-Abelian theory. It is obvious, that the model misses the very important aspect of confinement, and therefore might be of relevance at most for the case of heavy quarkonia. But even when disregarding the problems met already for QED in the above treatment, one should raise the question: How is it possible that the simplest model gives reasonable answers for the Abelian, but fails already in the lowest order of approximation for the non-Abelian theory? One realizes quickly that Eq. (5.9) by nature of its construction accounts at most for the electron positron, or more generally for the quark-antiquark kinetic energy and interaction, but certainly not for the gluon-gluon interactions. Therefore, the present procedure cannot be taken over to QCD without major modification.

VI. SUMMARY

As a particular example of applying the method of “discretized light-cone quantization” to quantum field theory in three space and one time dimension, we consider quantum electrodynamics and study the bound-state problem for positronium, particularly its Bohr-Sommerfeld aspects including the correct retardation and recoil structure.

The aim of the present work is rather modest. We want to see whether the continuum limit of discretized light-cone quantization exists, whether or not the numerical solutions are independent of formal parameters, and to which extent the solutions agree with available analytical work. Last but not least, we would like to provide the actual numbers. The aim is thus the technical question whether the method of DLCQ has a chance at all when applied to more difficult problems than positronium.

Summarizing the approach, the original DLCQ matrix equation is mapped identically onto another problem by a projector method. The so-obtained effective matrix equation is converted to an integral equation by going to the continuum limits. After two simplifying *ad hoc* assumptions, see Eq. (2.7), one arrives at the light-cone analogue of the Tamm-Dancoff equation, Eq. (2.14). The equation and the *ad hoc* assumptions are not particularly new; they had been used before in different contexts [6,13,14,15,19]. The main contribution of this work is the numerical solution of the Tamm-Dancoff equation in light-cone momenta, which has not been done so far, and its interpretation as an effective resummation to all orders. In addition, two other equations and their numerical solutions are studied in this work, the so-called light-cone Schrödinger equation and the usual Coulomb Schrödinger equation in momentum space, which both can be considered as non-relativistic approximations to the light-cone Tamm-Dancoff equation.

One should emphasize the effectivity of the numerical side of the approach. Most of the results have been generated by diagonalizing matrices as small as 225×225 . The so-called Coulomb counterterms which are applied here for the first time to gauge theory in light-cone coordinates are particularly important. They speed up convergence whenever one investigates numerically

Coulomb-like problems in the momentum representation and override some of our earlier pessimistic conclusions [9]. The numerical methods are also unexpectedly accurate. In order to extract reliably the hyperfine shift one needs at least ten significant figures.

Summarizing the numbers, one reproduces the expected Bohr spectrum $M_n = 2m [1 - B_n(\alpha^2/4)]$ almost quantitatively, as well as the typical relativistic effects such as the hyperfine shift $v = \alpha^4 C_{\text{hf}} m$. The binding coefficients $B_n \sim 1/n^2$ are reproduced with small but significant deviations. The discrepancies with the expected results are much smaller for the physical value $\alpha = 1/137$ than for $\alpha = 0.3$. Similarly, the hyperfine coefficient is close to the correct value $C_{\text{hf}} \sim 1/3$ for $\alpha = 1/137$, but for $\alpha = 0.3$ it is about twice as large. All of the results depend weakly on the value of the invariant momentum cutoff, with the tendency of overbinding. This seems to be caused by one identifiable term in the interaction. If one simply drops it according to Eq. (5.12), the results become much more satisfactory.

We have to conclude, therefore, particularly in view of having omitted important parts of the full theory as outlined in the preceding section, that the present work can only be an intermediate but important step in applying discretized light-cone quantization to three space and one time dimensions.

ACKNOWLEDGMENTS

We thank Stanley J. Brodsky and Andrew Tang from SLAC for many inspiring and encouraging discussions during all of this work. We also thank Roman Koniuk for sending us their explicit numerical results.

APPENDIX A: THE ELECTRON AND ITS MASS RENORMALIZATION

As in the positronium sector one separates the Fock space in the electron sector into a P - and a Q -space, $|e\rangle$ and $|e\gamma\rangle$, respectively. The P -space contains only two helicity states $s_e = \pm \frac{1}{2}$ of the electron with $x = 1$ and $\mathbf{k}_\perp = 0$; actually when using the point symmetries, it contains only one state. In Q -space, the electron states carry the quantum numbers $x', \mathbf{k}'_\perp, s_e$ and correspondingly the photon states $1 - x', -\mathbf{k}'_\perp, s_\gamma$. Since the P -sector contains only one state, the problem of solving the integral equation analogous to Eq. (2.14) reduces to the solution of an algebraic equation for the eigenvalue, i.e.,

$$m_F^2 + C + W(\omega) = \bar{M}_i^2(\omega) \quad \text{for } i = 1. \quad (\text{A1})$$

The LHS has contributions from the free part (m_F^2), from the contractions terms (C), and from the effective interaction $W(\omega) = VG(\omega)V$. The latter contains the vertex loop and describes the scattering of the electron from P -space into Q -space and back into P -space, as was displayed diagrammatically in Fig. 3. In principle one should calculate the resolvent $G(\omega)$ in Q -space. But since one should be consistent with the positronium sector, particularly Eq. (2.7), the inversion of the Hamiltonian in Q -space is trivial, i.e.,

$$G(\omega) = \frac{1}{\omega - M_{e\gamma}^2} = \left[\omega - \frac{m_F^2 + \mathbf{k}_1'^2}{x'} - \frac{\mathbf{k}_1'^2}{1-x'} \right]^{-1}. \quad (\text{A2})$$

The effective interaction is therefore

$$\begin{aligned} W(\omega) &= \sum_{s_e, s_\gamma} \int_D dx' d^2\mathbf{k}'_1 \langle e | V | e\gamma \rangle \langle e\gamma | V | e \rangle \frac{1}{\omega - M_{e\gamma}^2} \\ &= \frac{\alpha}{2\pi^2} \int_D dx' d^2\mathbf{k}'_1 \frac{1}{1-x'} \left[\frac{m_F^2(1-x')^2}{x'^2} \right. \\ &\quad \left. + \frac{\mathbf{k}_1'^2}{(1-x')^2} \left(\frac{1}{x'^2} + 1 \right) \right] \\ &\quad \times \frac{1}{\omega - M_{e\gamma}^2}, \end{aligned}$$

with the domain of integration D given by covariant Fock-space regularization, i.e.,

$$D: \frac{m_F^2 + \mathbf{k}_1'^2}{x'} + \frac{\mathbf{k}_1'^2}{1-x'} \leq \Lambda^2 + m_F^2. \quad (\text{A3})$$

Using the same model as above in Eq. (2.7), one gets, finally, with $\omega = \omega^* \equiv m_F^2$,

$$W = \frac{\alpha}{2\pi^2} \int_D dx' d^2\mathbf{k}'_1 \left[-\frac{2}{(1-x')^2} - \frac{1}{x'} + \frac{2m_F^2}{m_F^2(1-x')^2 + \mathbf{k}_1'^2} \right],$$

and

$$C = \frac{\alpha}{2\pi^2} \int_D dx' d^2\mathbf{k}'_1 \left[+\frac{2}{(1-x')^2} + \frac{1}{1-x'} \right], \quad (\text{A4})$$

where $W \equiv W(\omega^*)$. The contraction part C differs from the expressions in Table IX by the *regularization*, i.e., by restricting the domain of integration. The instantaneous photon part of the contractions [$\sim 2/(1-x')^2$] is then canceled exactly by the vertex loop. The instantaneous fermion part [$\sim 1/(1-x')$] does not cancel completely, and will contribute a logarithmically diverging piece. The sum $C + W \equiv \Delta m^2$ can be understood as the “self-mass (squared) correction” to the electron’s mass squared. With a notation reflecting the origin of terms, one obtains

$$\begin{aligned} \Delta m^2 &= \frac{\alpha}{2\pi^2} \int_D dx' d^2\mathbf{k}'_1 \left[\frac{2m_F^2(1+1-x')}{m_F^2(1-x')^2 + \mathbf{k}_1'^2} \right] \\ &= \frac{\alpha}{2\pi} m_F^2 \left[3 \ln \frac{\Lambda^2 + m_F^2}{m_F^2} - \frac{\Lambda^2}{m_F^2 + \Lambda^2} \right]. \quad (\text{A5}) \end{aligned}$$

Although the vertex loop and the contractions are quadratically divergent, the sum diverges only logarithmically with Λ , provided the vertex loop and the contractions are regulated consistently. In deriving this result, use was made of the identity

$$\begin{aligned} \int_D dx' d^2\mathbf{k}'_1 \frac{2m_F^2(1-x')}{m_F^2(1-x')^2 + \mathbf{k}_1'^2} \\ = \int_D dx' d^2\mathbf{k}'_1 \left[\frac{1}{1-x'} - \frac{1}{x'} \right], \end{aligned}$$

which however holds only for the domain as defined by Eq. (A3).

One should emphasize that the integral, Eq. (A5), agrees *exactly* with the perturbative and manifestly gauge-invariant expressions to order α , as obtained from the infinite-momentum frame [9] or from the Feynman rules [9,16], when the regulator Λ exceeds all limits and when the domain of integration becomes thus unlimited. The contraction terms are obviously necessary to obtain a gauge-invariant result.

The “in-medium electron regularization and renormalization” in the positronium sector proceeds correspondingly, as will be discussed shortly. The domain of integration is now given by

$$D: [m_F^2(x-x')^2 + (x\mathbf{k}'_1 - x'\mathbf{k}_1)^2] \frac{1}{x'(x-x')} \leq \Lambda^2.$$

With the symmetrized starting point energy ω^* as given by Eq. (2.7), the effective self-mass (squared) correction $\Delta M^2 = C + W(\omega^*)$ becomes

$$\begin{aligned} \Delta M^2 &= \frac{\alpha}{2\pi^2} \int_D dx' d^2\mathbf{k}'_1 \\ &\quad \times \left[\frac{2m_F^2}{m_F^2(x-x')^2 + (x\mathbf{k}'_1 - x'\mathbf{k}_1)^2} - \frac{1}{xx'} + \frac{1}{x(x-x')} \right]. \end{aligned}$$

Substituting $y = x'/x$ and $l = \mathbf{k}'_1 - y\mathbf{k}_1$ gives $\Delta M^2 = \Delta m^2/x$. For the further procedure one has two options: Either one fixes the electron mass $m_e^2 = m_F^2 + \Delta m^2$ (with $m_e = 511$ keV), or one adjusts the contraction terms C such that $\Delta m^2 = 0$ (with $m_F = 511$ keV). We have decided [9] for the latter: The contraction term C and the effective interaction $W(\omega^*)$ cancel each other exactly.

APPENDIX B: THE MATRIX ELEMENTS OF THE HAMILTONIAN

The matrix elements of the light-cone Hamiltonian have been derived earlier and can be found in Refs. [7,9,10]. For the sake of completeness, the explicit expressions are compiled in Tables VII–IX for the vertex V , the contraction C , and the seagull interaction S , respectively, to the extent they are needed in the present context. They hold for the continuum [7], as opposed to the discretized case [9]. The light-cone Hamiltonian $H_{\text{LC}} = T + V + S + C$ is the sum of these three interactions and of the free or “kinetic” energy:

$$T = \sum_{q_1} \left[\frac{m_F^2 + \mathbf{k}_1^2}{x} \right]_1 (b_1^\dagger b_1 + d_1^\dagger d_1) + \sum_{q_1} \left[\frac{\mathbf{k}_1^2}{x} \right]_1 a_1^\dagger a_1.$$

The creation operators b_q^\dagger , d_q^\dagger , and a_q^\dagger create plane-wave states for the electrons, positrons, and photons, respectively, characterized by the four kinematical quantum numbers $q \equiv (x, \mathbf{k}_1, \lambda)$, and the destruction operators b_q , d_q , and a_q destroy them correspondingly. They obey the usual (anti)commutation relations. Each single particle carries thus a longitudinal-momentum fraction x , transverse momentum \mathbf{k}_1 , and helicity λ . The fermions have mass m_F and kinetic energy $(m_F^2 + \mathbf{k}_1^2)/x$; the photons are massless. The symbol \sum_{q_1} denotes summation over the entire range of the quantum numbers. In the continuum limit sums are replaced by integrals, i.e., $\sum_{q_1} \rightarrow C_L \int dq_1$,

where

$$C_L \equiv \frac{\Omega P^+}{16\pi^3}$$

and

$$\int dq_1 \equiv \sum_{\lambda=\pm 1} \int_0^1 dx \int_{-\infty}^{+\infty} d(\mathbf{k}_1)_x \int_{-\infty}^{+\infty} d(\mathbf{k}_1)_y .$$

The normalization volume is denoted by $\Omega \equiv 2L_{\parallel}(2L_{\perp})^2$, and the total longitudinal momentum by P^+ . For notational reasons q is often suppressed, e.g., $a_1 \equiv a_{q_1}$, which should not be particularly confusing.

-
- [1] H. C. Pauli and S. J. Brodsky, Phys. Rev. D **32**, 1993 (1985).
- [2] H. C. Pauli and S. J. Brodsky, Phys. Rev. D **32**, 2001 (1985).
- [3] T. Eller, H. C. Pauli, and S. J. Brodsky, Phys. Rev. D **35**, 1493 (1987).
- [4] T. Eller and H. C. Pauli, Z. Phys. C **42**, 59 (1989).
- [5] K. Hornbostel, S. J. Brodsky, and H. C. Pauli, Phys. Rev. D **41**, 3814 (1990).
- [6] G. P. Lepage and S. J. Brodsky, Phys. Rev. D **22**, 2157 (1980).
- [7] G. P. Lepage, S. J. Brodsky, T. Huang, and P. B. Mackenzie, in *Particles and Fields—2*, Proceedings of the Banff Summer Institute, Banff, Canada, 1981, edited by A. Z. Capri and A. N. Kamal (Plenum, New York, 1983).
- [8] Th. Heinzl, St. Krusche, and E. Werner, Phys. Lett. B **256**, 55 (1991); Regensburg Report No. TPR91-20, 1991 (unpublished).
- [9] A. C. Tang, S. J. Brodsky, and H. C. Pauli, Phys. Rev. D **44**, 1842 (1991).
- [10] S. J. Brodsky and H. C. Pauli, Report No. SLAC-PUB-5558, 1991 (unpublished); in Proceedings of the 30th Schladming School in Particle Physics, 1991 (unpublished).
- [11] H. A. Bethe and E. E. Salpeter, *Quantum Mechanics of One- and Two-Electron Atoms* (Springer, Heidelberg, 1957).
- [12] G. T. Bodwin, D. R. Yennie, and M. A. Gregorio, Rev. Mod. Phys. **57**, 723 (1985).
- [13] D. Mustaki, S. Pinsky, J. Shigemitsu, and K. Wilson, Phys. Rev. D **43**, 3411 (1991); R. J. Perry, A. Harindranath, and K. G. Wilson, Phys. Rev. Lett. **65**, 2959 (1990).
- [14] I. Tamm, J. Phys. (U.S.S.R.) **9**, 449 (1945).
- [15] S. M. Dancoff, Phys. Rev. **78**, 382 (1950).
- [16] M. Kaluza, Ph.D. thesis, Heidelberg, 1990.
- [17] L. C. L. Hollenberg, K. Higashijima, K. R. C. Warner, and B. H. J. McKellar, Report No. KEK-90-186, 1991 (unpublished).
- [18] P. M. Morse and H. Feshbach, *Methods in Theoretical Physics* (McGraw-Hill, New York, 1953), Vols. 1 and 2.
- [19] S. J. Brodsky and G. P. Lepage, in *Perturbative Quantum Chromodynamics*, edited by A. H. Mueller (World Scientific, Singapore, 1989), p. 93.
- [20] M. Sawicki, Phys. Rev. D **32**, 2666 (1985); **33**, 1103 (1986).
- [21] G. Hardekopf and J. Sucher, Phys. Rev. A **30**, 703 (1984).
- [22] H. C. Pauli, Z. Phys. A **319**, 303 (1984).
- [23] W. Hackbusch, *Integralgleichungen* (Teubner, Stuttgart, 1989).
- [24] K. A. Atkinson, *A Survey of Numerical Methods for the Solution of Fredholm Integral Equations of the Second Kind* (Society of Industrial and Applied Mathematics, Philadelphia, PA, 1976).
- [25] A. H. Stroud and D. Secrest, *Gaussian Quadrature Formulae* (Prentice Hall, Englewood Cliffs, NJ, 1966).
- [26] J. R. Spence and J. P. Vary, Phys. Rev. D **35**, 2191 (1987).
- [27] O. Nachtmann, *Elementarteilchenphysik* (Vieweg, Braunschweig, 1986).
- [28] J. Björken and S. Drell, *Relativistic Quantum Mechanics* (McGraw-Hill, New York, 1964); *Relativistic Quantum Fields* (McGraw-Hill, New York, 1965).
- [29] L. Manciewicz (private communication).
- [30] K. Alder and R. M. Steffen, in *The Electromagnetic Interaction in Nuclear Spectroscopy*, edited by W. D. Hamilton (North-Holland, Amsterdam, 1975), p. 1.
- [31] W. Dykshoorn, R. Koniuk, and R. Muñoz-Tapia, Phys. Rev. A **41**, 60 (1990).
- [32] W. Dykshoorn and R. Koniuk, Phys. Rev. A **41**, 64 (1990).
- [33] T. Kinoshita and G. P. Lepage, in *Quantum Electrodynamics*, edited by T. Kinoshita (World Scientific, Singapore, 1990).
- [34] H. C. Pauli, Nucl. Phys. A **369**, 413 (1981).
- [35] M. Krautgärtner, Ph.D. thesis, University of Heidelberg, 1992.